Photoelectrochemistry of Heterointerfaces for Solar Fuels

.

Stefano Caramori

Dipartimento di Scienze Chimiche e Farmaceutiche ed Agrarie dell'Università di Ferrara

What we do

Transparent Photoelectrochemical Cells

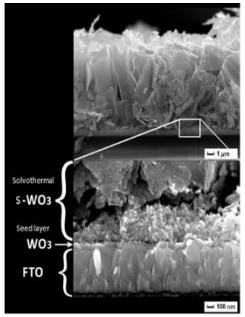

Photoelectrodes for water splitting, solar fuel production and environmental remediation

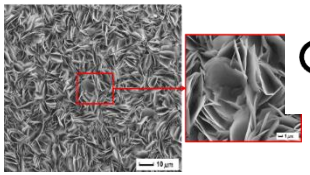

Photocatalysis for pollutant degradation

Electrocatalysts for CO_2 reduction

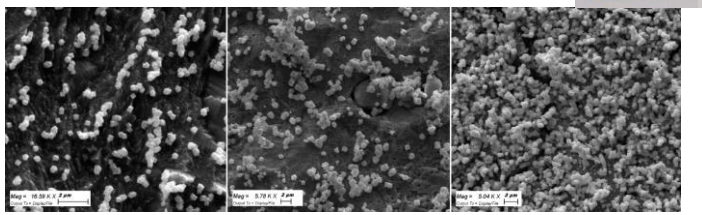

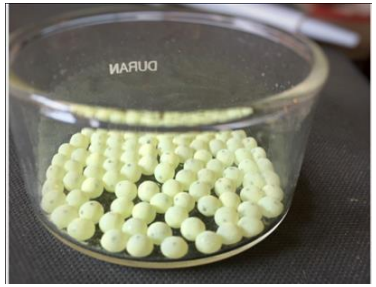

Marie Curie "Arcadia" (H2020-MSCA-IF 2015)

CARIPLO « ECONOMIA CIRCOLARE: RICERCA PER UN FUTURO SOSTENIBILE»: *CO2 Enrich» 2021-2024 (with Statale di Milano and Milano Bicocca)*

Horizon Europe SOREC2 (2022-2025) https://cordis.europa.eu/project/id/101084326

Content

- Electron levels in semiconductors and some photoelectrochemistry concepts
- Case studies about charge transfer processes at modified interfaces
- Conclusions, consequences and applications

Artificial photosynthesis via photoelectrochemical cells

In a photoelectrosynthetic cell: either hydrogen or carbon dioxide reduction product could be obtained. Hydrogen is «easy», selective reduction of CO_2 is also feasible but more challenging due to several reaction pathways

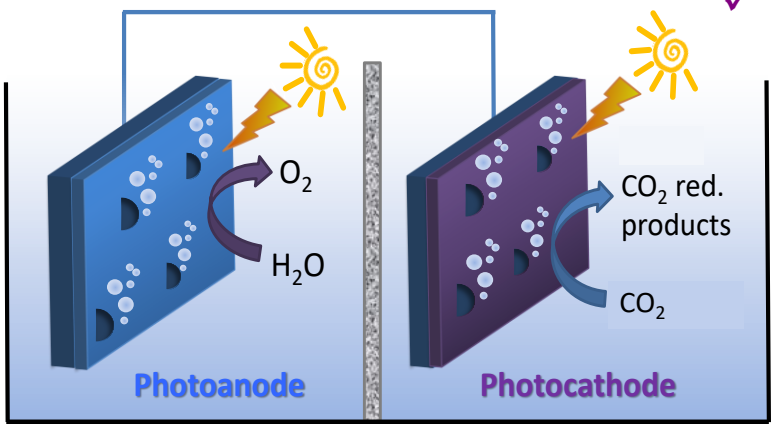

✓ **Several possible reduction semireactions:**

$$CO_2 + 2H^+ + 2e^- \rightarrow HCO_2H$$
$$CO_2 + 2H^+ + 2e^- \rightarrow CO + H_2O$$
$$2CO_2 + 2H^+ + 2e^- \rightarrow H_2C_2O_4$$
$$CO_2 + 4H^+ + 4e^- \rightarrow HCHO + H_2O$$
$$CO_2 + 6H^+ + 6e^- \rightarrow CH_3OH + H_2O$$
$$CO_2 + 8H^+ + 8e^- \rightarrow CH_4 + 2H_2O$$

at the (photo)**cathode**

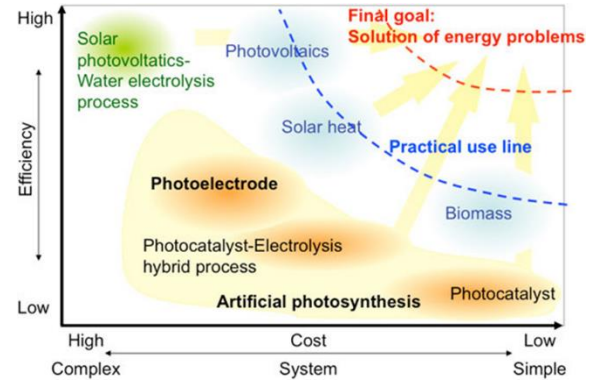

✓ **Oxidation semireaction:**

$$2\,H_2O \rightarrow 4\,H^+ + 4\,e^- + O_2$$

at the (photo)**anode**

✓ **Value-added products**

✓ **Closing the CO_2 cycle**

OER as a key step to solar fuels

Journal of Catalysis 396 (2021) 192–201
Contents lists available at ScienceDirect
Journal of Catalysis
journal homepage: www.elsevier.com/locate/jcat

Importance of the oxyl character on the IrO_2 surface dependent catalytic activity for the oxygen evolution reaction

Danilo González [1], Javier Heras-Domingo [1], Mariona Sodupe, Luis Rodríguez-Santiago, Xavier Solans-Monfort *

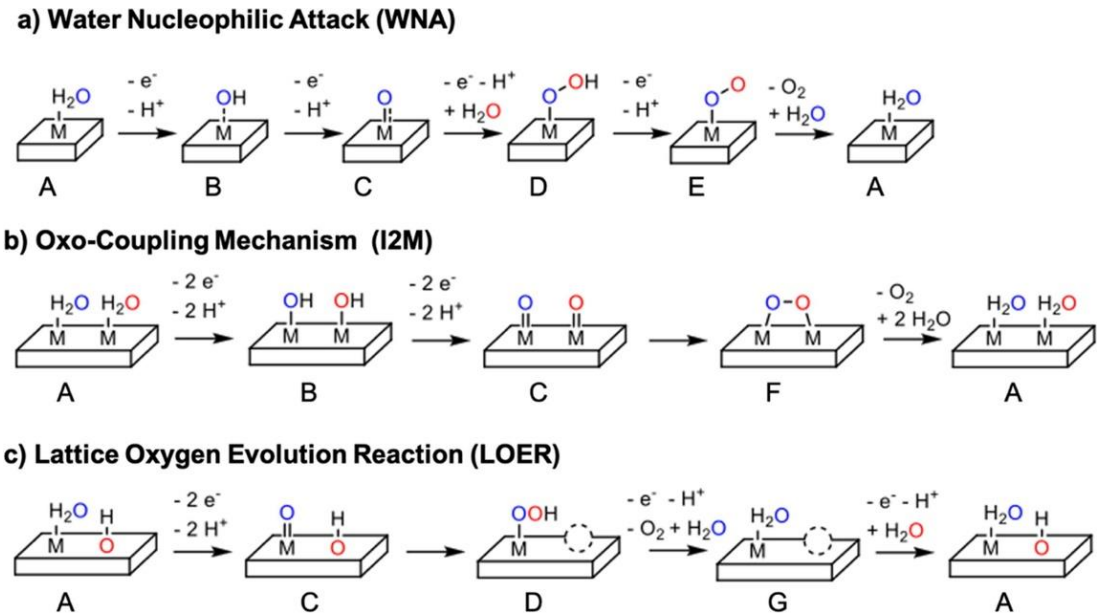

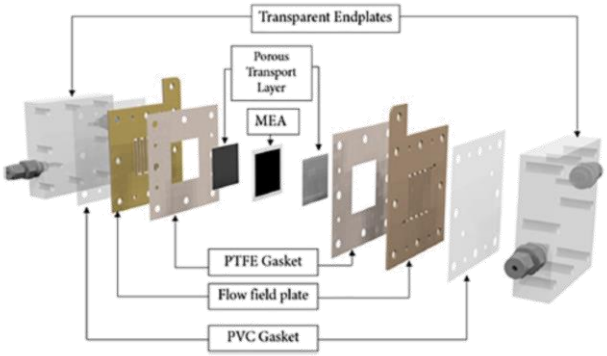

FIGURE 1 | Schematic of the PEMWE cell used for the study.

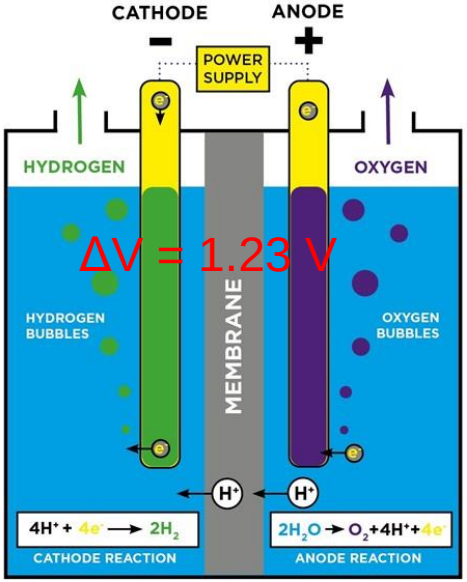

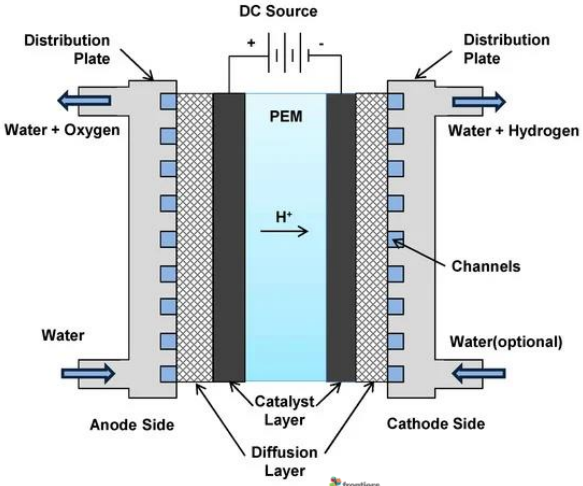

frontiers in Energy Research

Optimisation of Mass Transport Parameters in a Polymer Electrolyte Membrane Electrolyser Using Factorial Design-of-Experiment

Jude O. Majasan, Jason I. S. Cho, Maximilian Maier, Paul R. Shearing and Dan J. L. Brett*
Electrochemical Innovation Lab, Department of Chemical Engineering, University College London, London, United Kingdom

energies
MDPI
Article

Generic Dynamical Model of PEM Electrolyser under Intermittent Sources

Sumit Sood [1,*], Om Prakash [1], Mahdi Boukerdja [1], Jean-Yves Dieulot [1], Belkacem Ould-Bouamama [1], Mathieu Bressel [2] and Anne-Lise Gehin [1]

Solar Radiation Spectrum

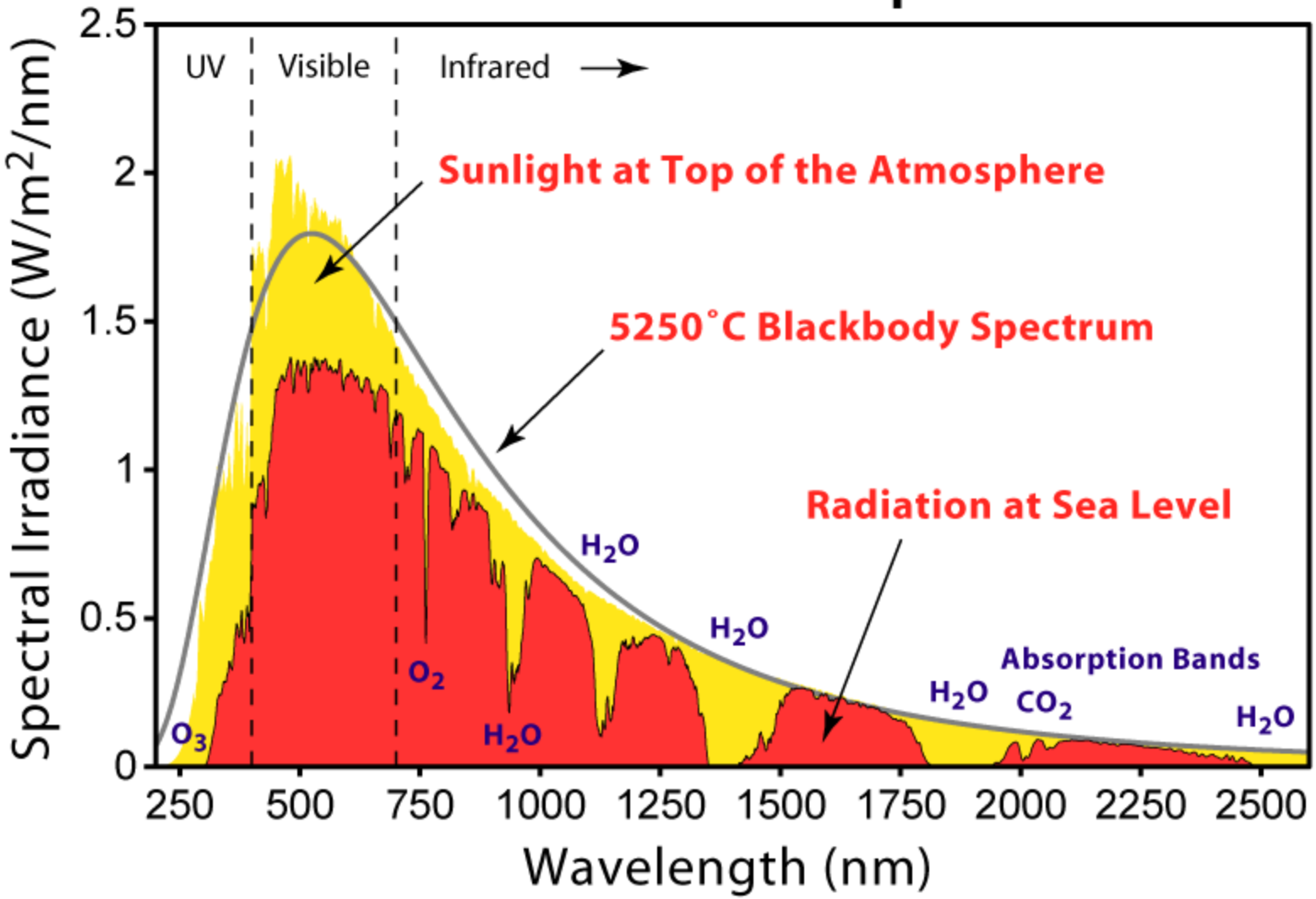

Typical n-type PEC Current/Voltage characteristic: **voltage saving with respect to conventional electrolysis**

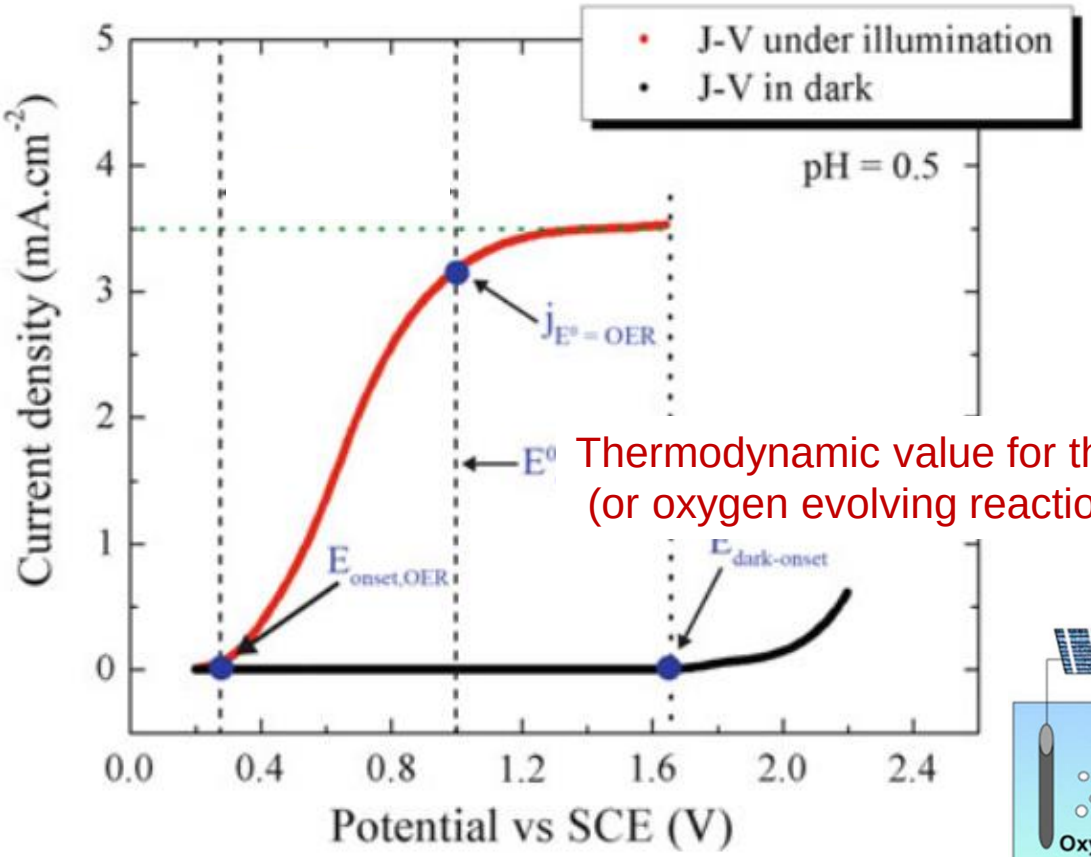

Thermodynamic value for the water oxidation (or oxygen evolving reaction, OER) at pH 0.5, vs SCE

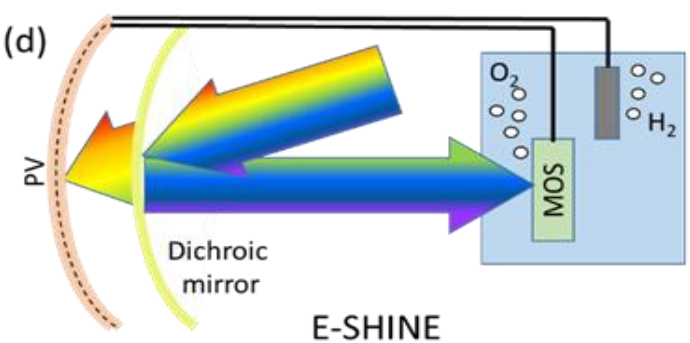

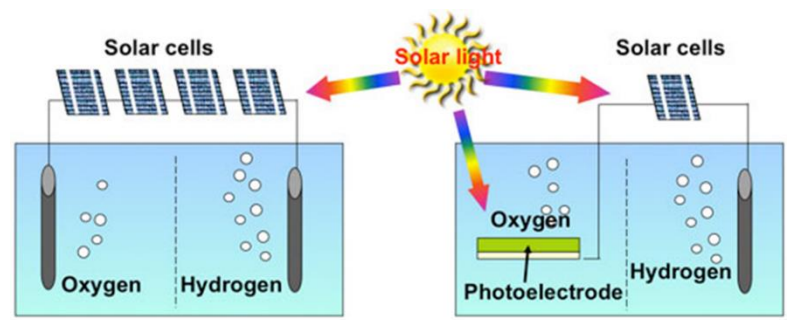

Hydrogen production by normal water electrolysis using solar cells
*Including overvoltage more than 1.6 V of electrolysis voltage is needed.
(4 solar cells in series)

Hydrogen ptoduction using photoelectrode
*Number of solar cells can be reduced because the voltage of auxiliary power supply can be reduced.

Total production cost can be reduced than the normal water electrolysis using solar cells.

Photocurrent Generation

$$J(x) = n(x)\mu_n(x)(\nabla U(x) + \nabla \mu(x))$$

J (x) = carrier flux

n(x)= carrier concentration

$\mu_n(x)$ Mobility (velocity/field)

$\nabla U(x)$ Electric potential gradient (electric field) (drift/migration)

$\nabla \mu(x)$ Chemical potential gradient (diffusion)

Either or just one of these fields give rise to the flow of carriers which trigger photoelectrochemical reactions at the interfaces of the PEC

A more complete view of energy levels in real solids

Fig. 2.6 Energy levels of shallow and deep donors (SD, DD) and acceptors (SA, DA) in a semiconductor. Deep donor or acceptor states can also occur below or above midgap, respectively. Midgap states (RC) are often very efficient recombination centers and can be either donor- or acceptor-like in nature

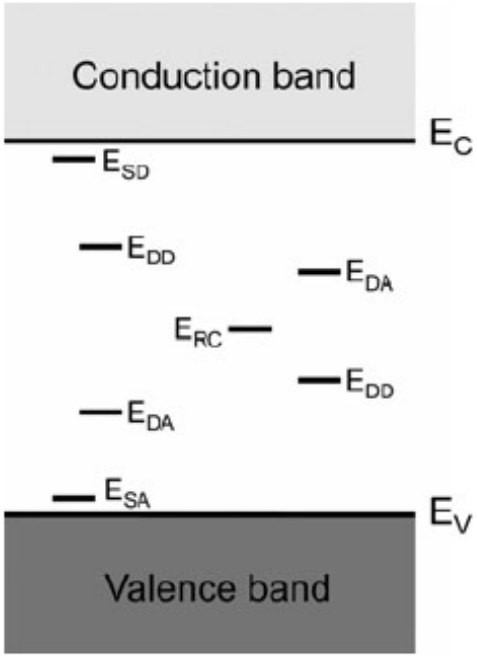

Formation of Semiconductor/electrolyte Junction (Schottky model)

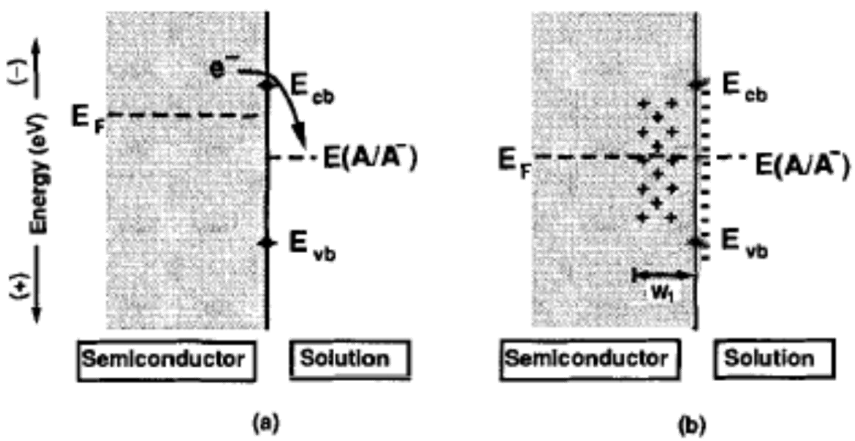

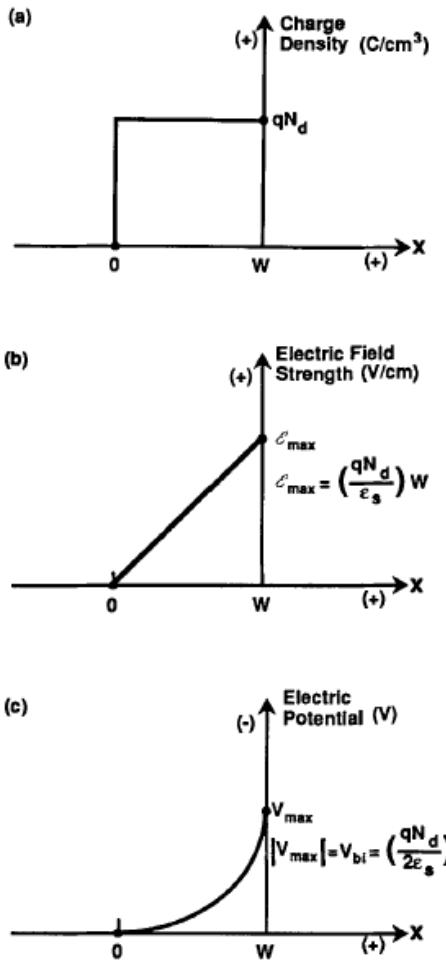

Poisson equation under strong field conditions

.

$$-\frac{\partial^2 V}{\partial x^2} = \frac{qN_{D^+}}{\varepsilon}$$

$$W = \sqrt{\frac{2\,\varepsilon_s V_{bi}}{qN_d}}$$

Principles and Applications of Semiconductor Photoelectrochemistry

MING X. TAN, PAUL E. LAIBINIS, SONBINH T. NGUYEN, JANET M. KESSELMAN, COLBY E. STANTON, *and* NATHAN S. LEWIS*

Division of Chemistry and Chemical Engineering
California Institute of Technology
Pasadena, California

Figure 11. The spatial dependence of the charge density, the electric field, and the electric potential in the semiconductor at equilibrium. The origin of the *x*-axis (the distance axis) is chosen for convenience as the point where the net charge density in the semiconductor becomes zero. (*a*) The distance dependence of the charge density under the depletion approximation. (*b*) The electric field strength as a function of distance. Note that the maximum electric field strength occurs at the semiconductor/liquid interface. (*c*) The distance dependence of the electric potential in the semiconductor. The electric potential in the bulk of the semiconductor has been defined to be zero. Because the sign of the electric field strength is positive, the electric potential at the interface is more negative than it is in the bulk.

Semiconductor/Electrolyte interface

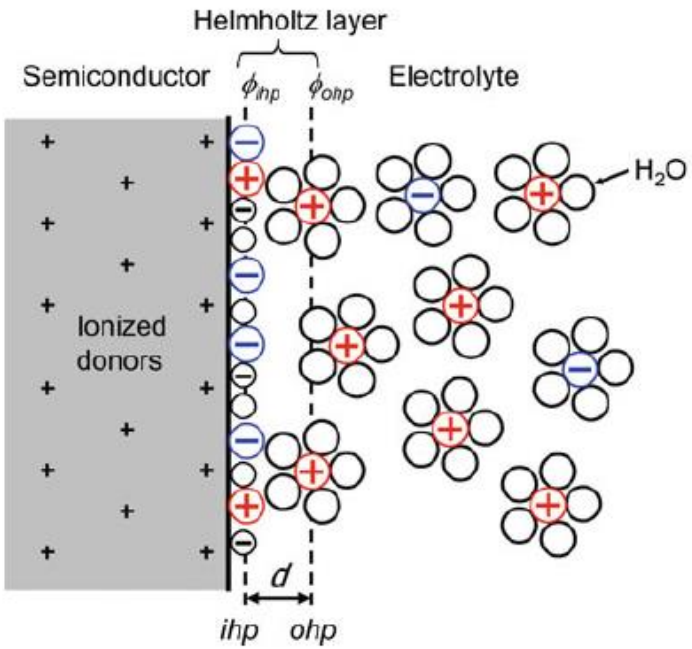

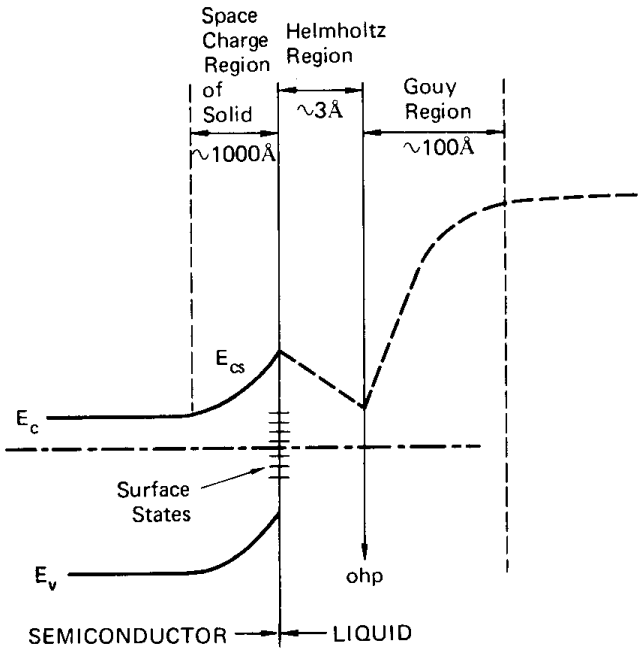

Figure 2.2. Double layers at the solid/liquid interface. The dashed line through the liquid indicates the variation in potential energy of a unit negative charge, as determined only by the double layer voltages, as it moves from the conduction band of the solid into the solution. The Gouy layer thickness indicated would represent a very dilute solution (Section 2.2.2).

Electrochemistry at Semiconductor and Oxidized Metal Electrodes

S. Roy Morrison

SRI International (formerly Stanford Research Institute) Menlo Park, California

J-V characteristic under illumination: n-type SC

$$J = J_{photo} - J_0\left(e^{\frac{-qV}{kT}} - 1\right)$$

$$J_{photo} \propto \phi_0 \alpha e^{-\alpha x}$$

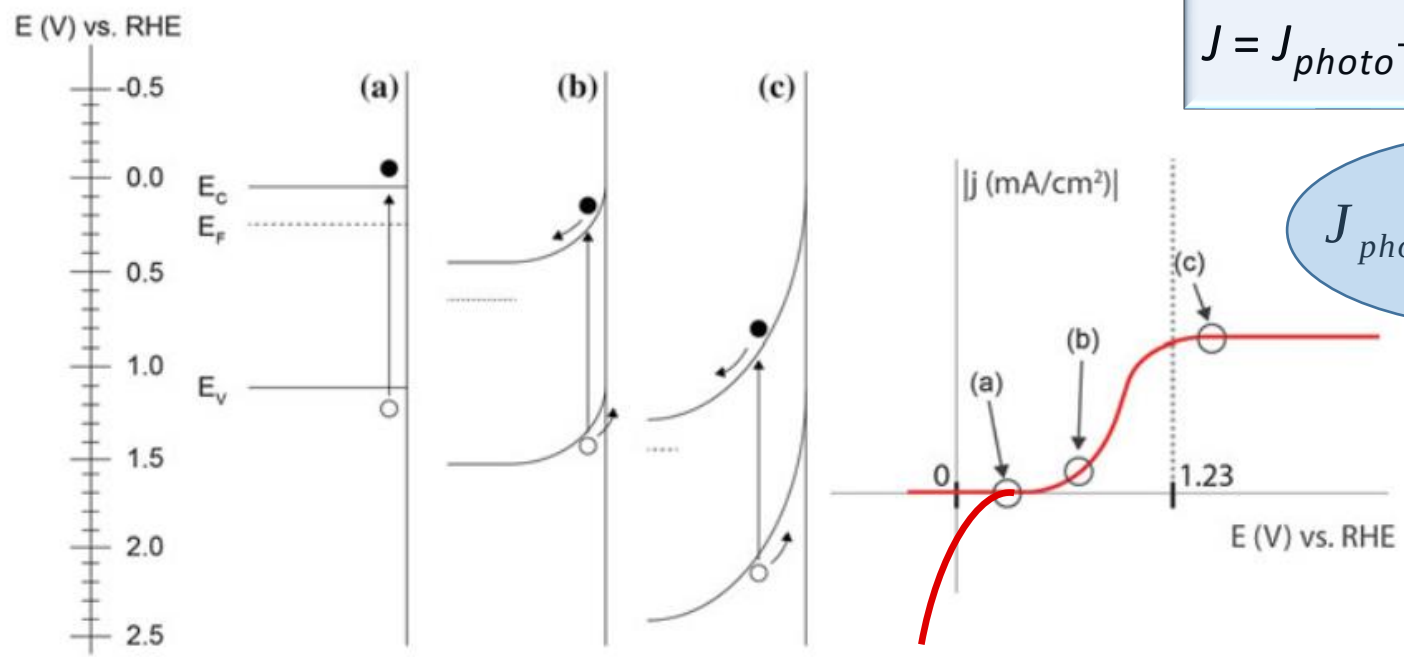

Fig. 6.7 Band diagram of a n-type photoanode at (**a**) flat-band potential, (**b**) a potential sufficient to separate charge carriers and drive photocurrent, and (**c**) large reverse bias potential sufficient to saturate the photocurrent response. The corresponding hypothetical *j–V curve* is shown on the *right*

Photovoltage and quasi-Fermi levels

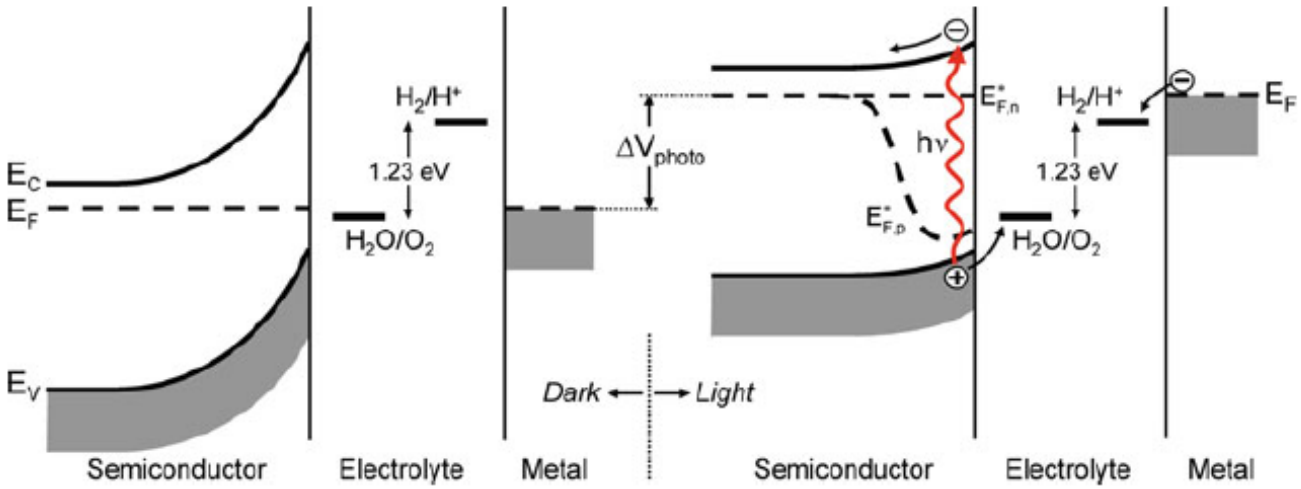

Fig. 2.20 Band diagram for a PEC cell based on an n-type semiconducting photoanode that is electrically connected to a metal counter electrode; in equilibrium in the dark (*left*) and under illumination (*right*). Illumination raises the Fermi level and decreases the band bending. Near the semiconductor/electrolyte interface, the Fermi level splits into quasi-Fermi levels for the electrons and holes

$$\varepsilon_{F(SC)} = \varepsilon_C - kT\ln\left(\frac{N_C}{n}\right), \qquad \varepsilon_{F(SC)} = \varepsilon_V + kT\ln\left(\frac{N_V}{p}\right)$$

$${}_n\varepsilon_F^* = \varepsilon_C - kT\ln\left(\frac{N_C}{n^*}\right) = \varepsilon_{F(SC)} + kT\ln\left(\frac{n+\Delta n^*}{n}\right)$$

$${}_p\varepsilon_F^* = \varepsilon_V + kT\ln\left(\frac{N_V}{p^*}\right) = \varepsilon_{F(SC)} - kT\ln\left(\frac{p+\Delta p^*}{p}\right)$$

SEMICONDUCTORS for PEC DEVICE

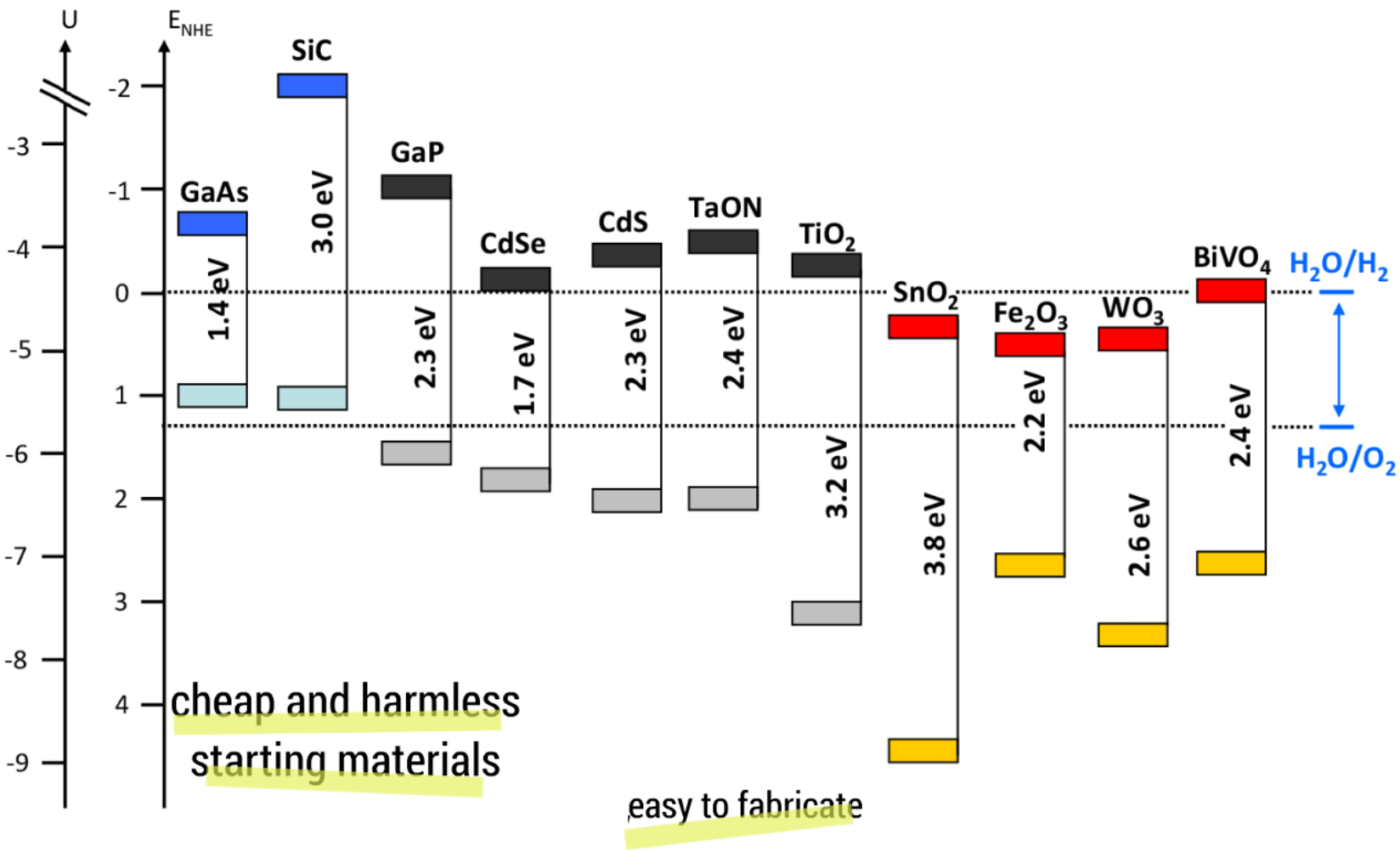

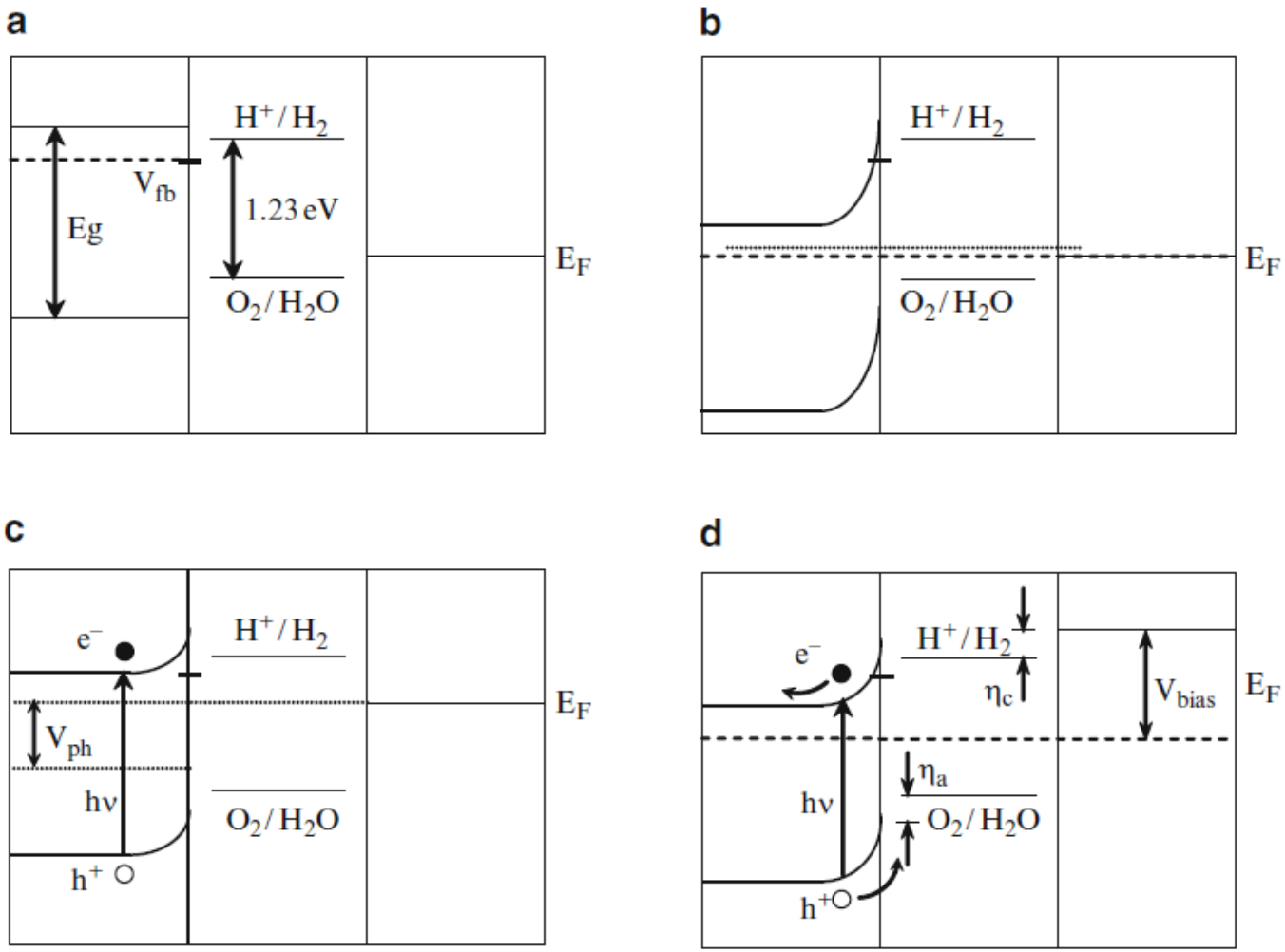

Fig. 3 Energy level diagrams for a semiconductor-metal photoelectrolysis cell: (**a**) no contact, (**b**) equilibrium in the dark, (**c**) high intensity irradiation, (**d**) high intensity irradiation with anodic bias

Some tandem PEC configurations

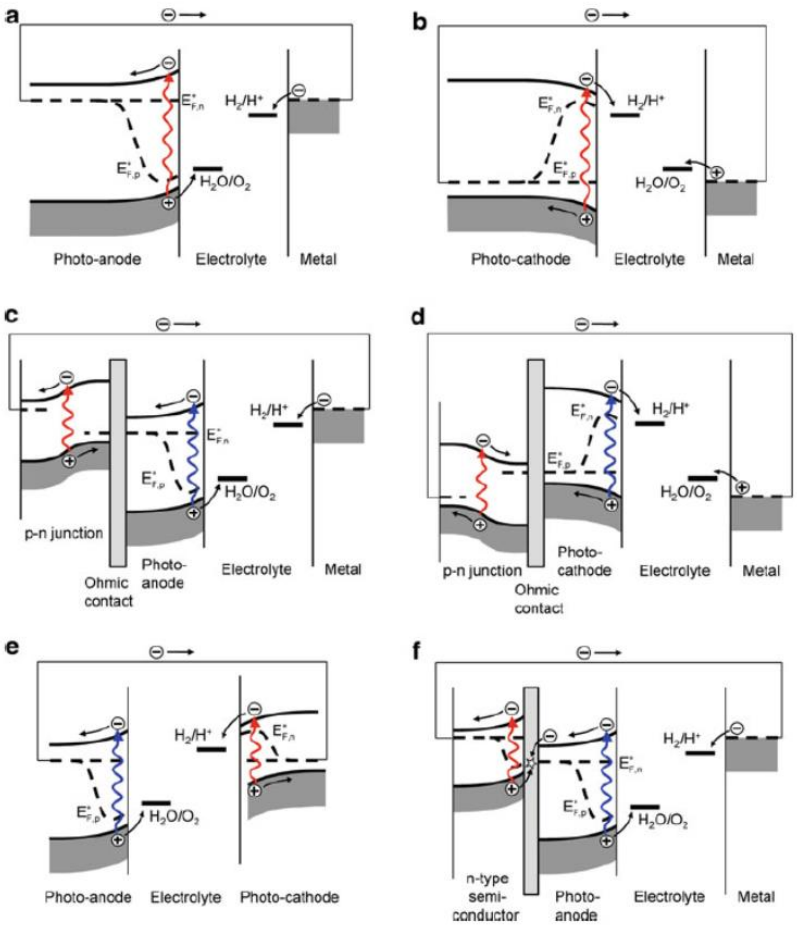

Fig. 2.25 Examples of possible PEC configurations under illumination. *Top row*: Standard single-semiconductor devices based on a photoanode (**a**) or photocathode (**b**) with a metal counter electrode. *Middle row*: Monolithic devices based on a photoanode (**c**) or photocathode (**d**) biased with an integrated p–n junction. *Bottom row*: p–n junction photoelectrochemical device (**e**), and an n–n heterojunction PEC device based on a photoanode deposited on top of a second n-type semiconductor that "boosts" the energy of the electrons (**f**)

nature photonics LETTERS
PUBLISHED ONLINE: 11 NOVEMBER 2012 | DOI: 10.1038/NPHOTON.2012.265

Highly efficient water splitting by a dual-absorber tandem cell

Jeremie Brillet[1], Jun-Ho Yum[1], Maurin Cornuz[1], Takashi Hisatomi[1], Renata Solarska[2], Jan Augustynski[2], Michael Graetzel[1] and Kevin Sivula[1]*

"Water splitters fabricated using triple-junction amorphous silicon1,2 or III–V3 semiconductors have demonstrated reasonable efficiencies, but at high cost and high device complexity"

More on STH

$$\mathrm{STH} = \left[\frac{(\mathrm{mmol\ H_2/s}) \times (237{,}000\ \mathrm{J/mol})}{P_{\mathrm{total}}\ (\mathrm{mW/cm^2}) \times\ \mathrm{Area}\ (\mathrm{cm^2})}\right]_{\mathrm{AM1.5\ G}}$$

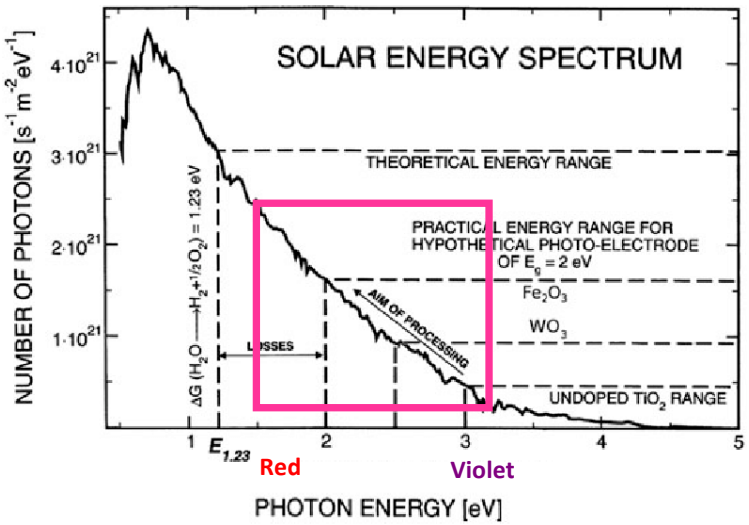

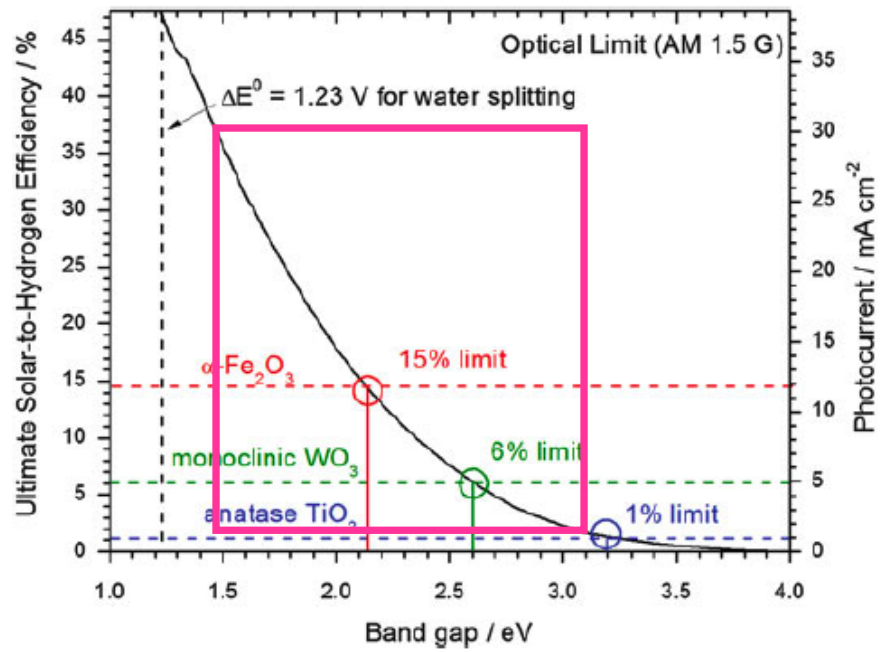

Fig. 1.2 Theoretical maximum solar-to-hydrogen (STH) conversion efficiency (*left axis*) and photocurrent (*right axis*) as a function of material band gap.

Nanostructured Materials

GOOD PROPERTIES

- Active Surface
- low T, wet routes available
- Diffusion Length

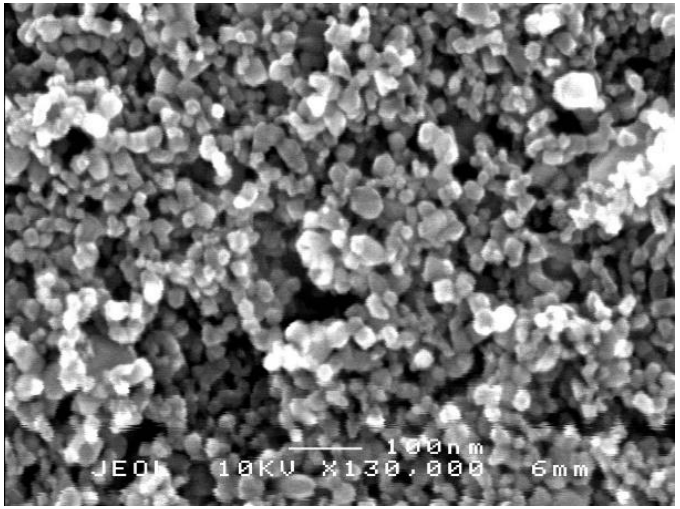

Sol-gel TiO_2

Drawbacks

- Defects/SS
- Traps

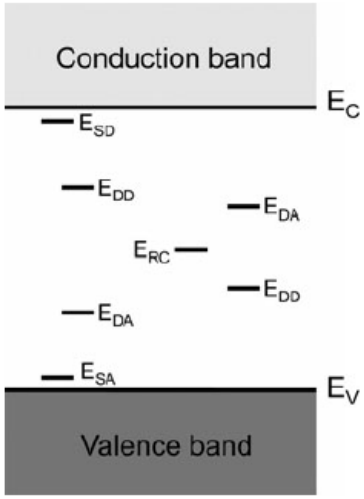

Tuning the surface properties with “catalytic” layers

➢ **Catalytic layers as SCs overcoatings**

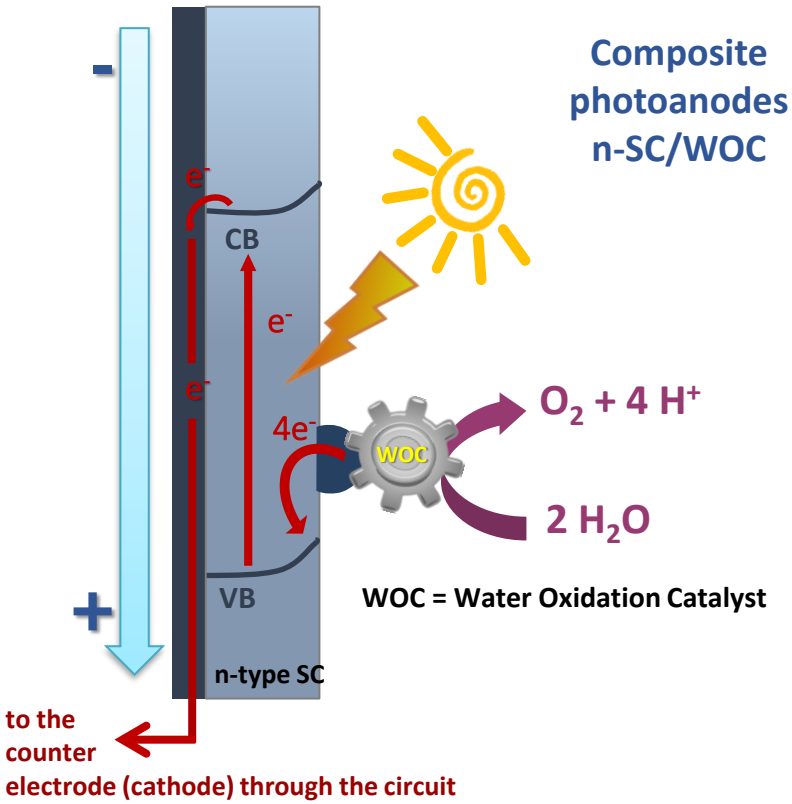

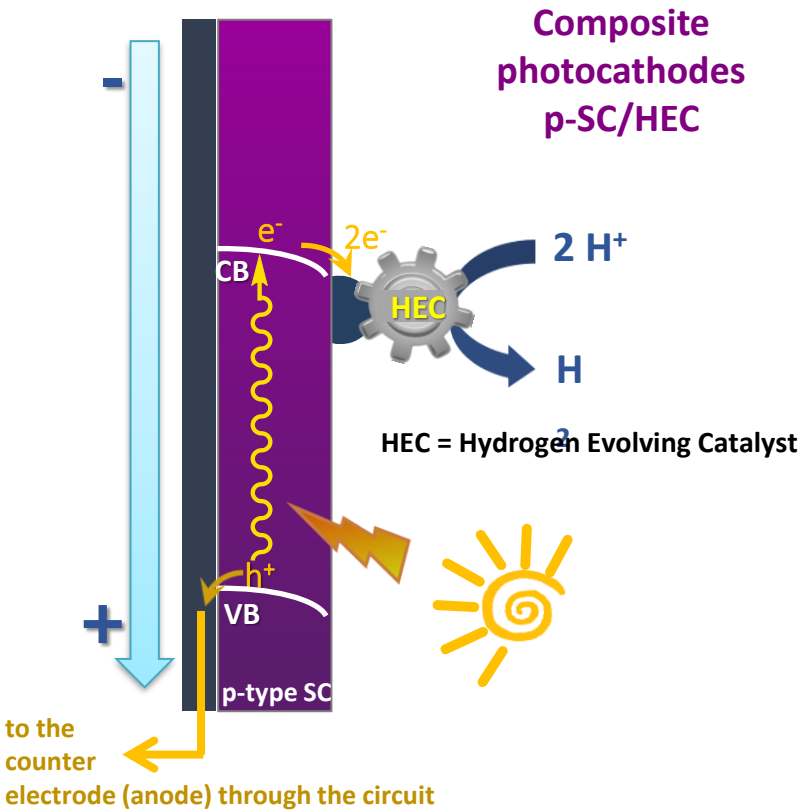

HEMATITE

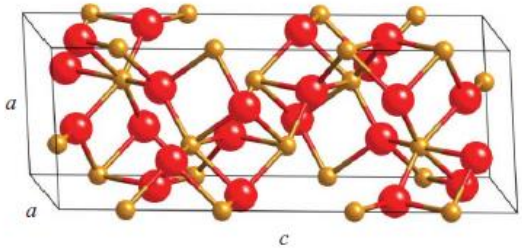

fast electron/hole recombination

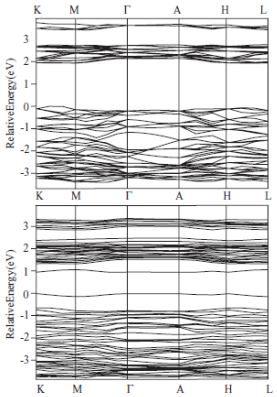

FIG. 11. The band structures for pure hematite (upper) and 8% Pd-doped (lower) are plotted across high-symmetry directions in the Brillouin zone. Here, we use the conventions K = (1/3, 1/3, 0), M = (1/2, 0, 0), Γ = (0, 0, 0), A = (0, 0, 1/2), H = (1/3, 1/3, 1/2), and L = (1/2, 0, 1/2). The zero of energy in each case is the energy of the highest occupied band.

low hole mobility (L_D 2-4 nm)

low electronic conductivity

high number of traps

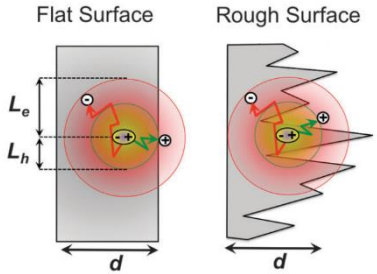

1. **nanostructuring**
2. **doping**

slow hole/interfacial transfer kinetics (0.001 - 1 ms timescale)

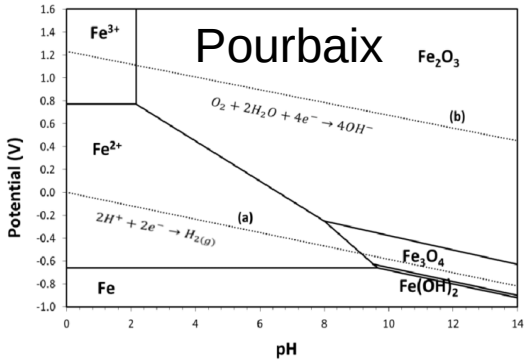

3. **surface modification**

Amorphous Fe(III) oxide as a water oxidation catalyst

PCCP RSCPublishing

PAPER

Cite this: *Phys. Chem. Chem. Phys.*, 2013, **15**, 13083

Efficient solar water oxidation using photovoltaic devices functionalized with earth-abundant oxygen evolving catalysts†

Vito Cristino,[a] Serena Berardi,[b] Stefano Caramori,*[a] Roberto Argazzi,[b] Stefano Carli,[a] Laura Meda,[c] Alessandra Tacca[c] and Carlo Alberto Bignozzi*[a]

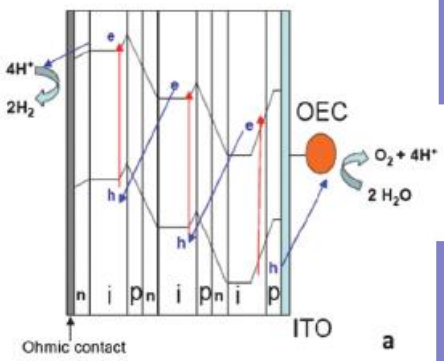

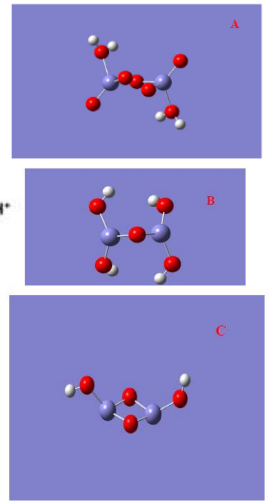

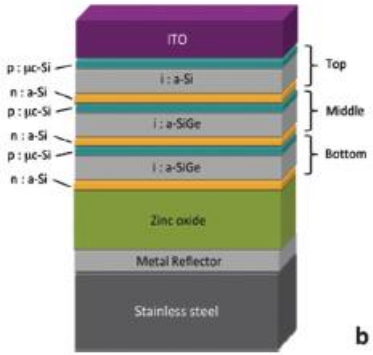

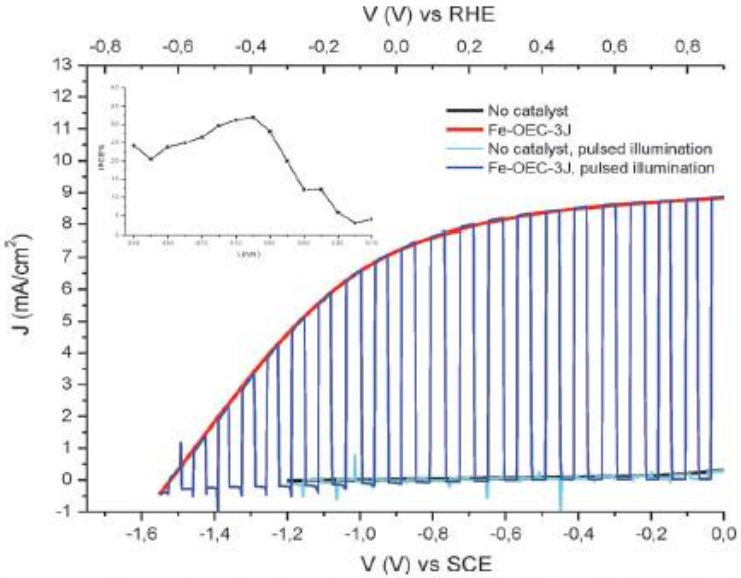

Fig. 7 *J–V* curves recorded under AM 1.5 G illumination in 0.5 M Na_2CO_3 (pH 11.2). The 3J cell (either modified with Fe-OEC or unmodified) is used as the photoanode in a three electrodes cell. Inset: photoaction spectrum of Fe-OEC-3J in a three electrodes cell, recorded in 0.5 M Na_2CO_3 (pH 11.2) at 0 V *vs.* SCE.

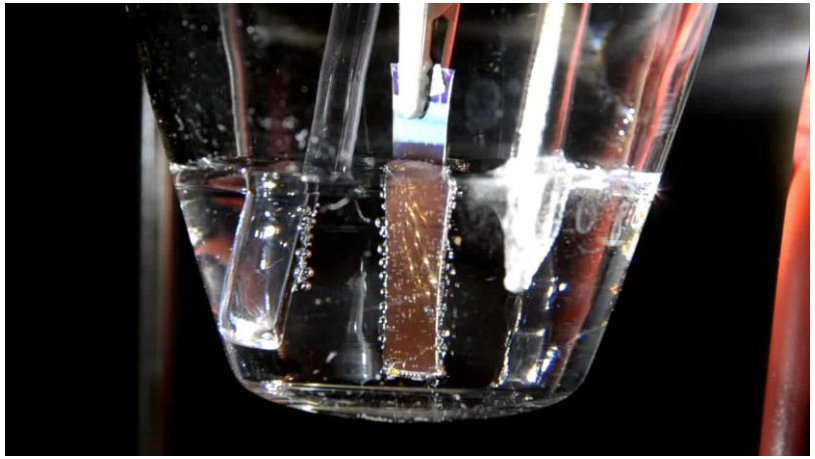

1- HYDROTHERMAL SYNTHESIS OF HEMATITE THIN FILM

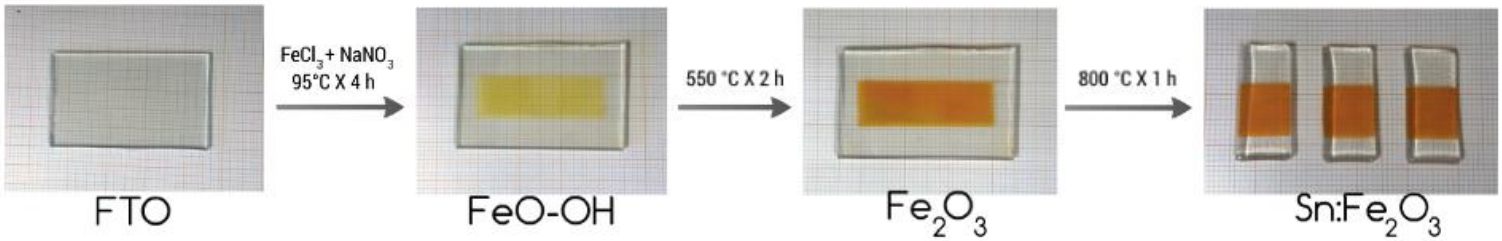

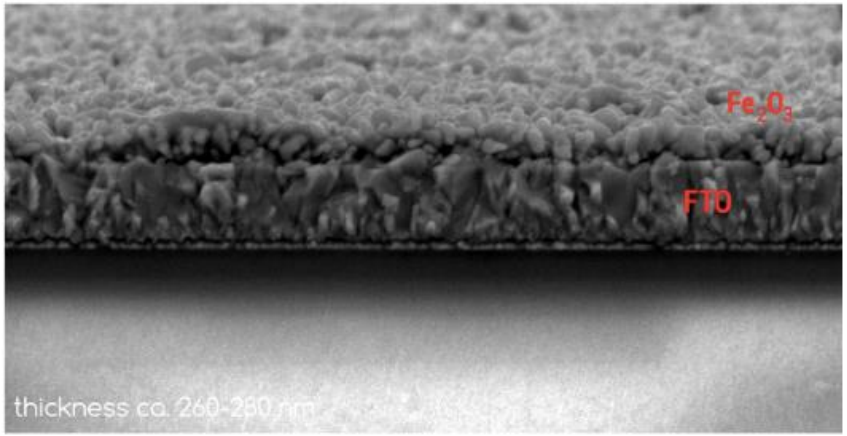

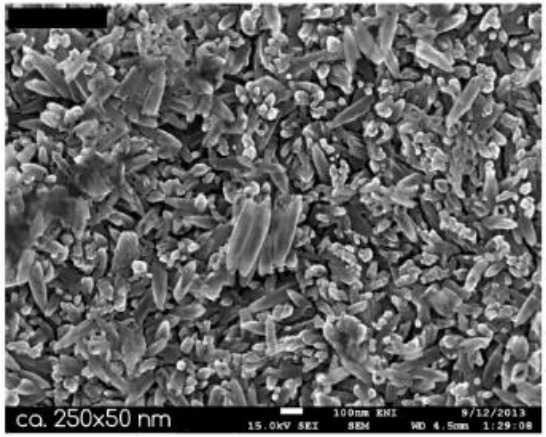

CHEMPHYSCHEM ARTICLES
ChemPubSoc Europe
DOI: 10.1002/cphc.201301143

Hematite Photoanodes Modified with an Fe^{III} Water Oxidation Catalyst

Nicola Dalle Carbonare,[a] Vito Cristino,[a] Serena Berardi,[b] Stefano Carli,[a] Roberto Argazzi,[b] Stefano Caramori,*[a] Laura Meda,[c] Alessandra Tacca,[c] and Carlo Alberto Bignozzi*[a]

Dedicated to Prof. Michael Grätzel on the occasion of his 70th birthday

2- SILAR DEPOSITION OF Fe-OEC

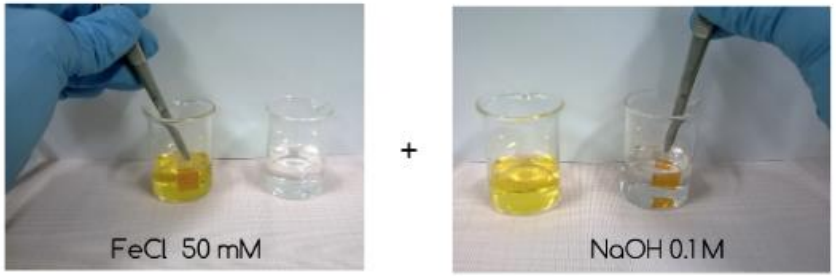

x 10 times

200°C x 20'

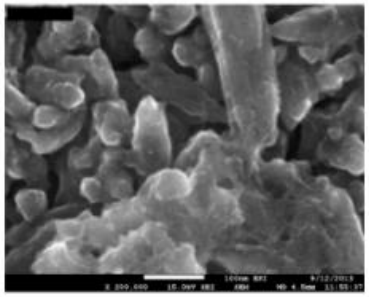

Photoelectrochemical behavior of Fe-OEC modified interface

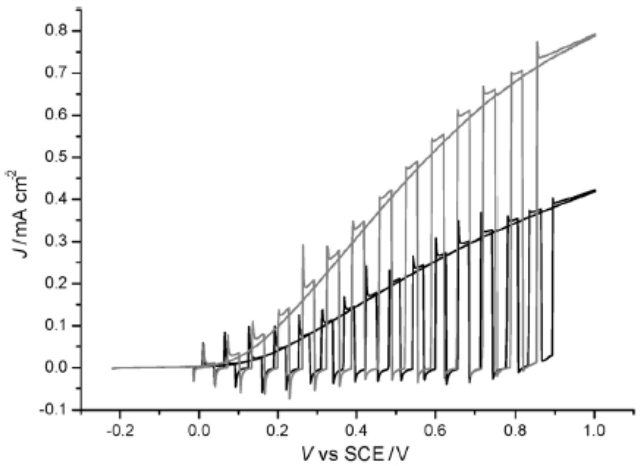

Figure 3. *J–V* curves under continuous and shuttered illumination (AM 1.5 G) of Fe-OEC-modified hematite (grey line) compared to the unmodified hematite (black line) in 0.5 M sodium borate buffer (pH 11.5).

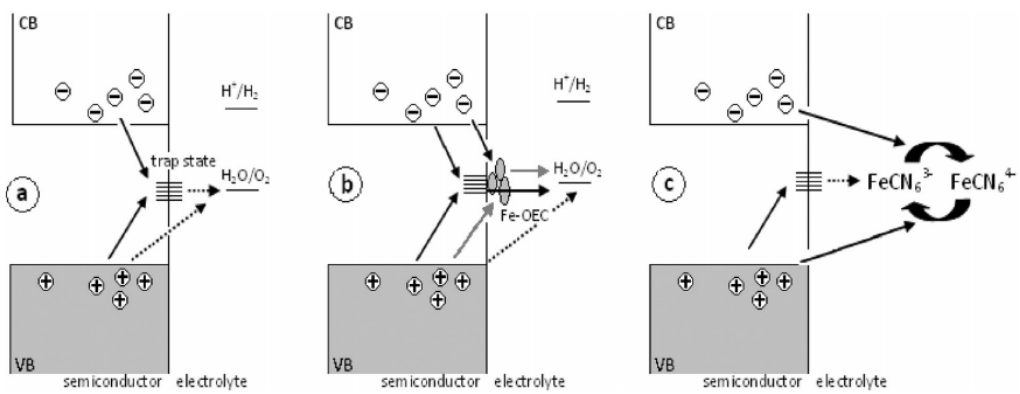

Scheme 1. Charge-transfer and recombination pathways hypothesized on the basis of photovoltage decay experiments. In unmodifed hematite (a), holes are prevailingly trapped in intraband gap states, where they slowly recombine with electrons (dark solid lines). In the Fe-OEC-modified hematite (b), holes are partly scavenged by the surface-bound catalyst either via trap states (dark solid lines) or by direct transfer from the valence band (grey lines) (VB). Recombination involves both holes trapped in the catalyst and in trap states. In the presence of a reversible redox shuttle (Fe^{II}/Fe^{III}) (c), holes trapped in intraband states or in the VB react with Fe^{II} forming Fe^{III}. Electrons recombine with Fe^{III} resulting in fast photovoltage decay.

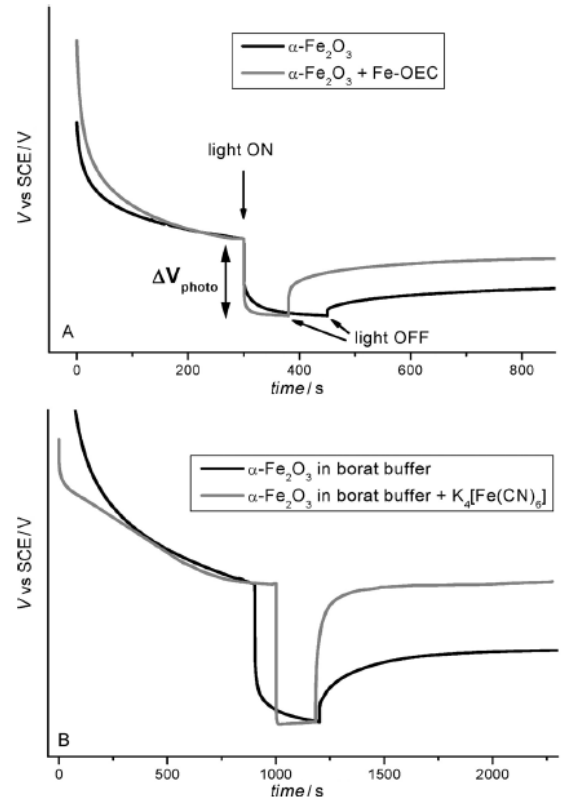

Figure 5. Open-circuit photovoltage decays of: A) unmodified hematite (black line) and Fe-OEC-modified hematite (same electrode after functionalization) (grey line) in 0.5 M sodium borate buffer (pH 11.5); B) unmodified hematite in the absence and in the presence of 0.1 M $K_4[Fe(CN)_6]$ in sodium borate buffer (pH 11.5). For the sake of clarity, in all cases ΔV_{photo} was normalized to the same value.

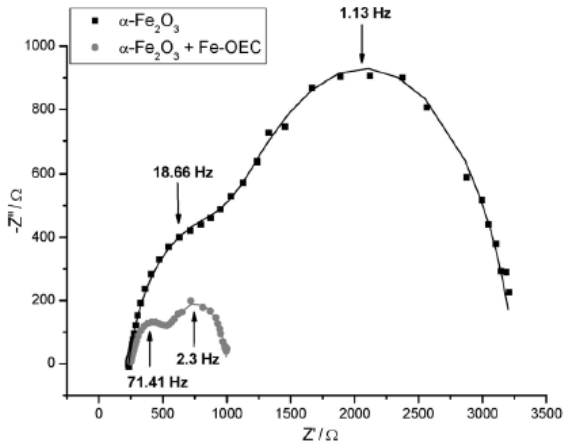

Figure 6. Complex plane plot (0.3 V vs. SCE) of the same hematite electrode before (black squares) and after (grey circles) functionalization with Fe-OEC under AM 1.5 G illumination in 0.5 M sodium borate buffer (pH 11.5). The data are fitted (solid line) with the model reported in Scheme 2.

Scheme 2. Equivalent circuit used for fitting the EIS data.

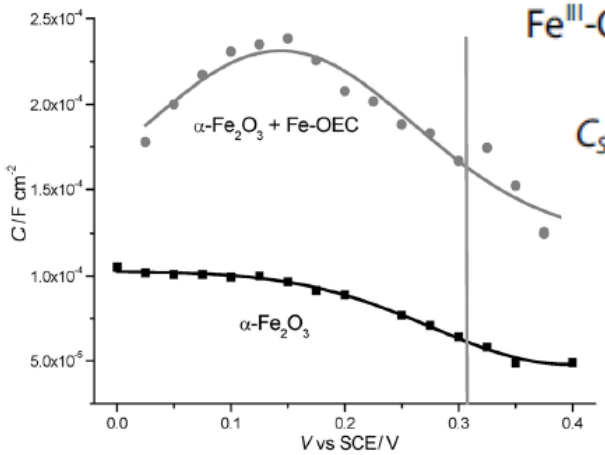

Figure 9. Capacitance of the semiconductor/electrolyte interface under AM 1.5 G illumination (100 mW cm^{-2}) of the same hematite electrode before (black squares) and after (grey circles) surface modification with Fe-OEC measured in 0.5 M sodium borate buffer (pH 11.5). The grey bar indicates the thermodynamic potential for oxygen evolution.

$$Fe^{III}\text{-}OH + h^+ \rightarrow Fe^{IV} = O + H^+$$

$$C_{SS} = e^2 \frac{N_{SS}}{kT} \frac{\exp\left(\frac{E_{SS}-\mu}{kT}\right)}{\left[\exp\left(\frac{E_{SS}-\mu}{kT}\right)+1\right]^2}$$

« ….the interfacial behavior is dominated by hole trapping in surface states, which are believed to be the intermediates responsible for the OER. The considerable increase in the surface trap capacitance in the presence of FeOEC indicates a favorable transfer of holes to the catalyst, which, being an amorphous hydrated oxide, easily undergoes PCET allowing the long lived storage of oxidizing equialvents in reactive states exposed to the electrolyte »

Ti(IV) modified hematite interfaces

ACS APPLIED MATERIALS & INTERFACES
www.acsami.org Research Article

Better Together: Ilmenite/Hematite Junctions for Photoelectrochemical Water Oxidation

Serena Berardi, Jagadesh Kopula Kesavan, Lucia Amidani, Elia Marek Meloni, Marcello Marelli, Federico Boscherini, Stefano Caramori, and Luca Pasquini*

Cite This: ACS Appl. Mater. Interfaces 2020, 12, 47435−47446 Read Online

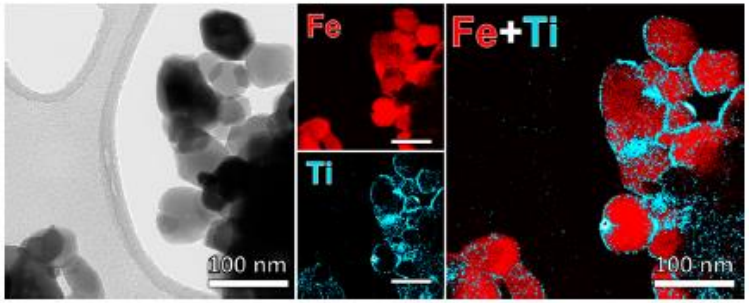

Figure 6. TEM micrographs of MPH_5Ti, related ESI Fe and Ti maps, and the combined map.

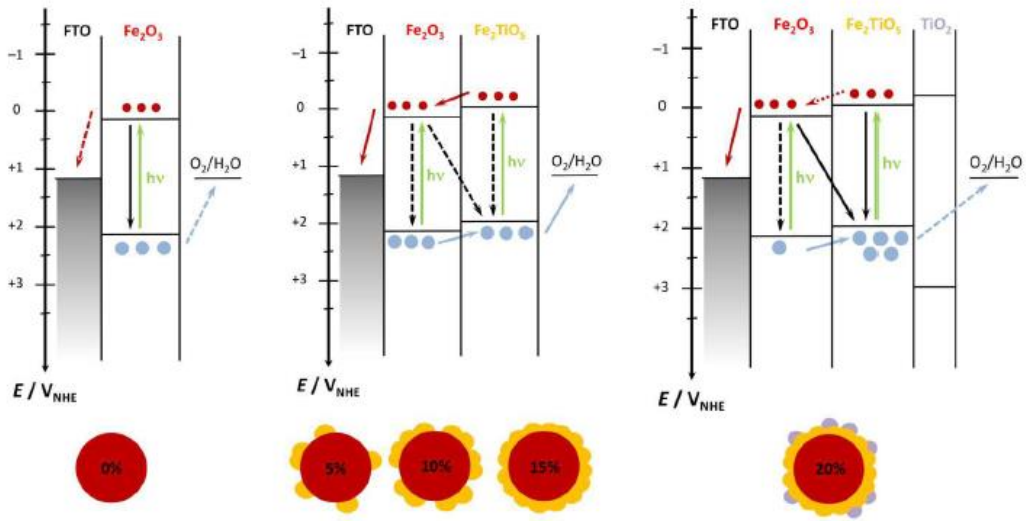

Energy Environ. Sci., 2015,**8**, 3242-3254

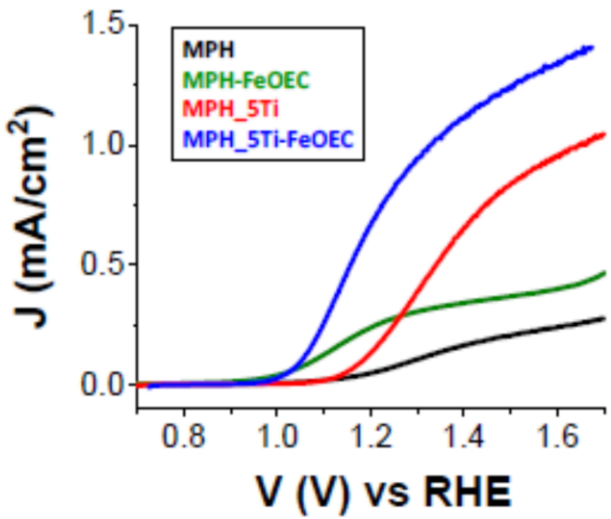

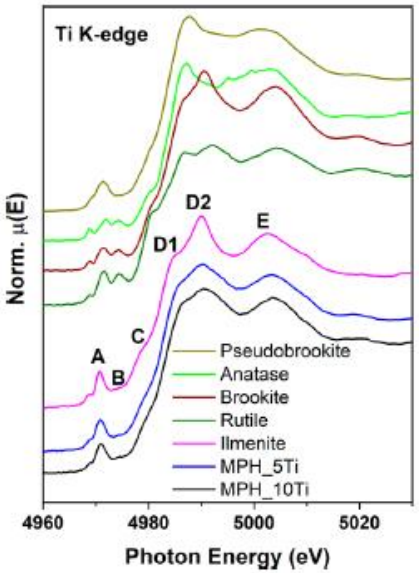

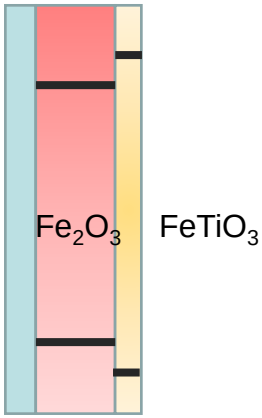

Figure 2. Ti K edge normalized XANES spectra of Ti-modified MPH compared to pseudobrookite, anatase, brookite, rutile, and ilmenite reference spectra.

Transient Optical Absorption in semiconductors: a simplified view

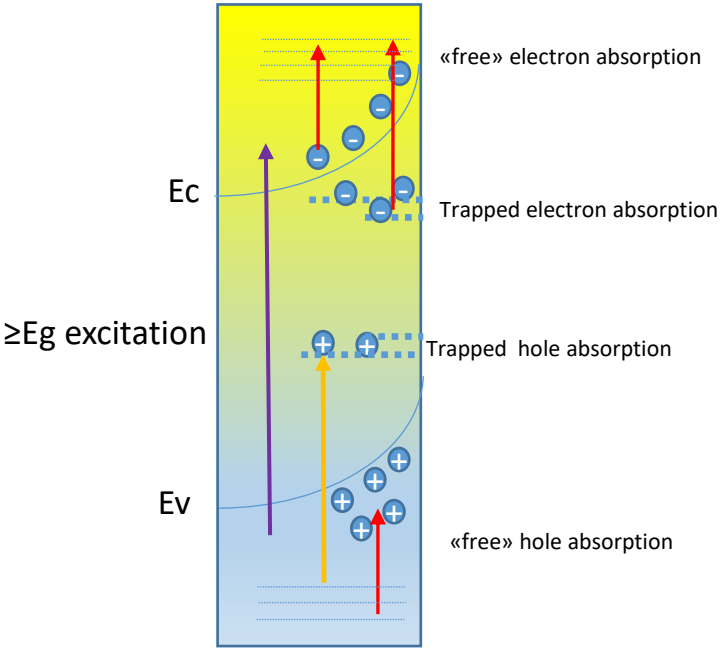

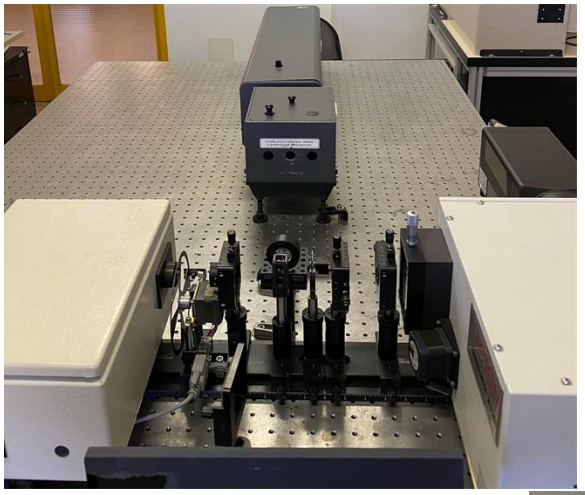

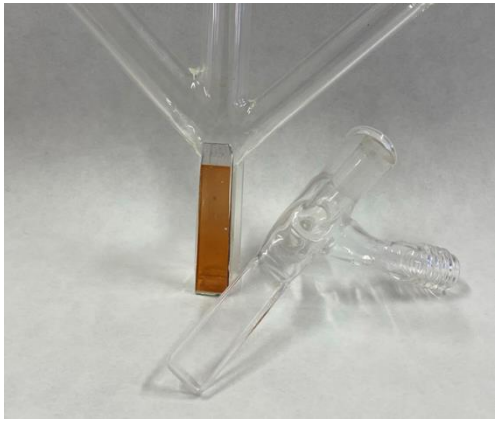

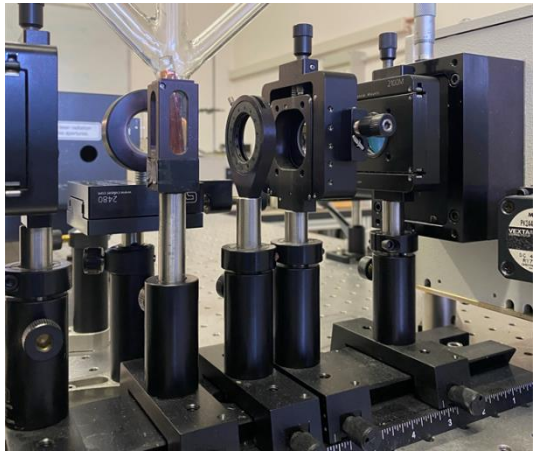

Transient Spectroscopy of Ti-modified hematite

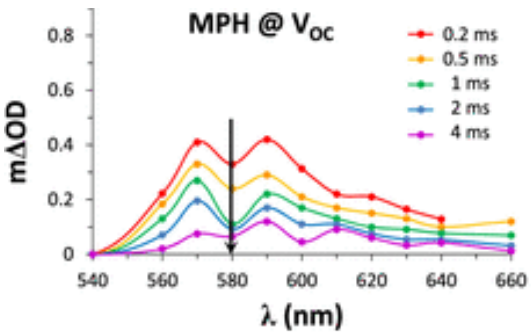

A

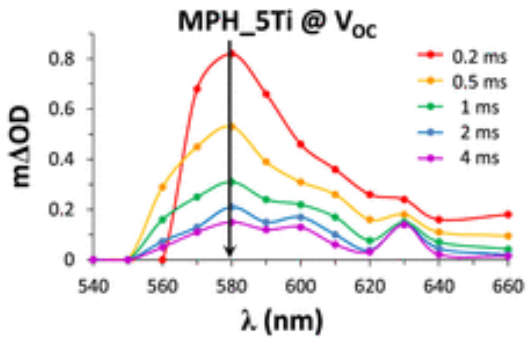

B

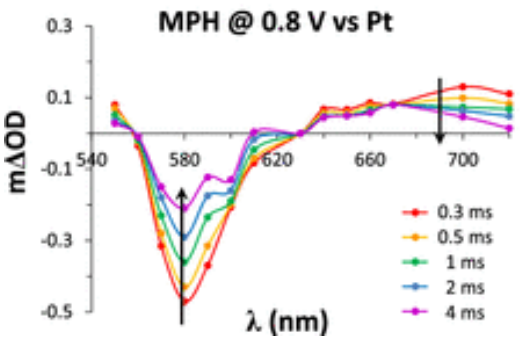

C

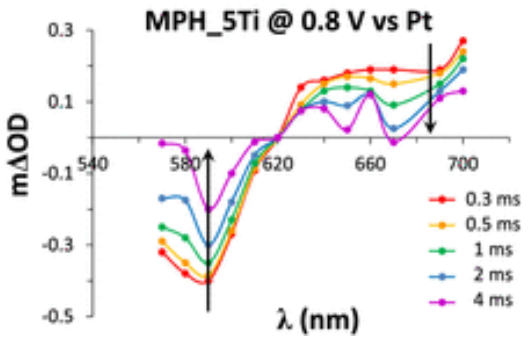

D

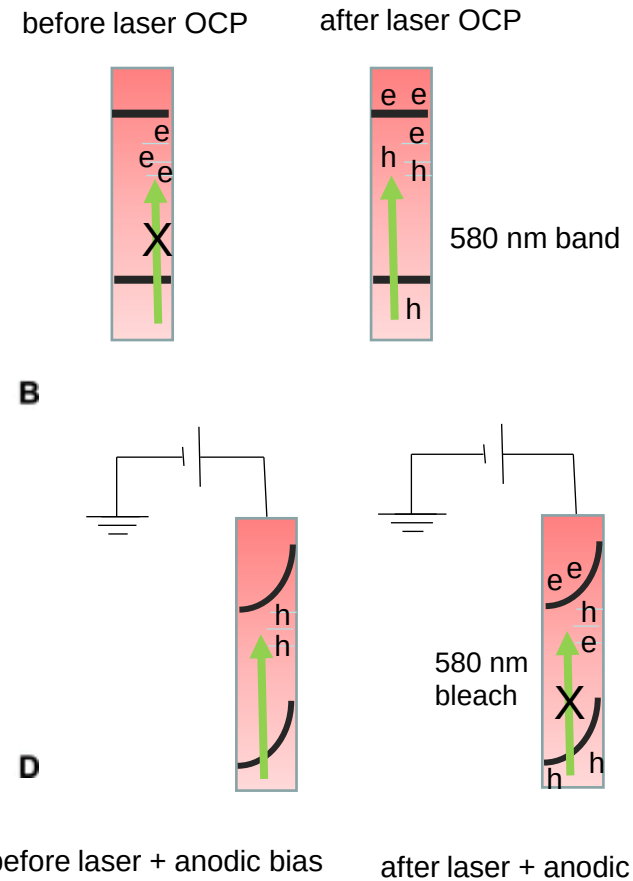

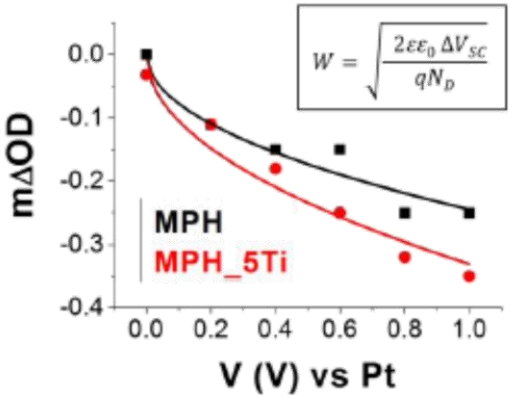

J. Durrant et al.

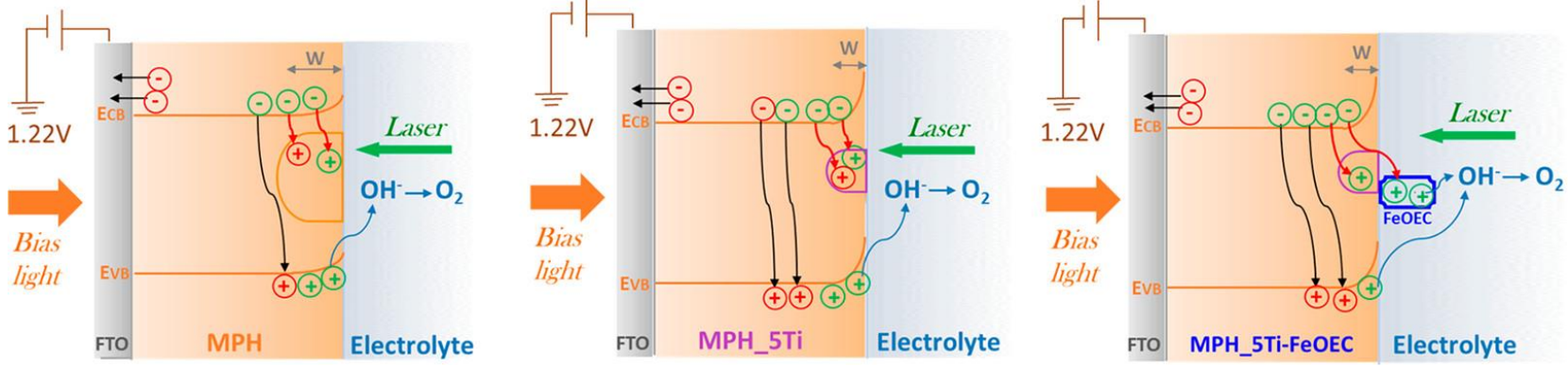

Ilmenite overlayer eliminates electron traps and unpins hematite Fermi level from traps, allowing for a stronger depletion layer to form. FeOEC improves Interfacial charge transfer

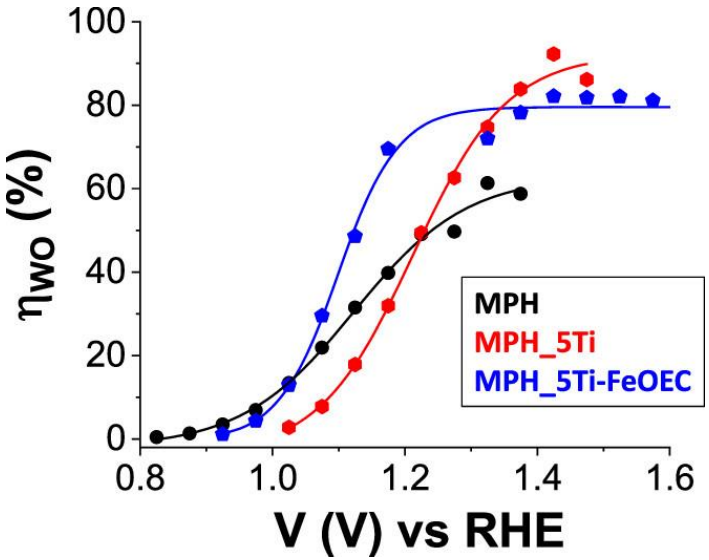

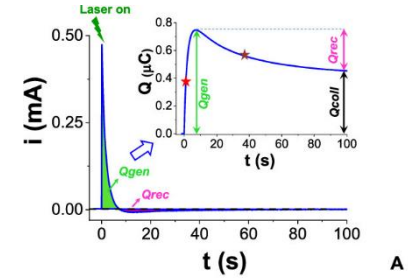

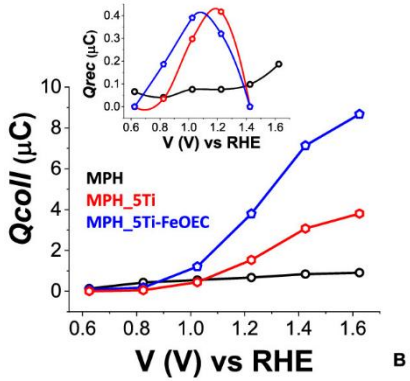

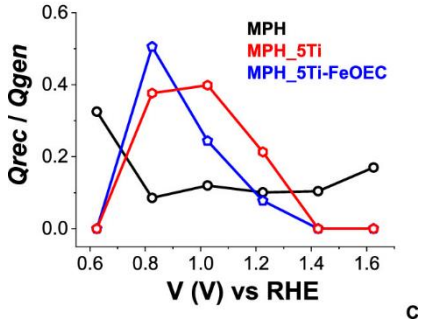

Capitalizing Hematite Photoanodes for Biomass Oxidation

Deng *et al*. hydrothermal synthesis to produce nanostructured thin films of hematite

- Variation of time, temperature and pressure
- Additives in the autoclave solution
- Seedlayers/underlayers

Can affect the **thickness** and the **morphological growth** of hematite film

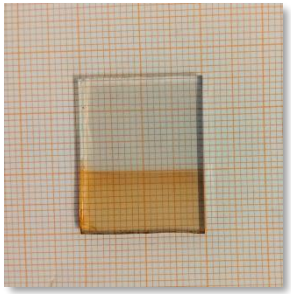

1st step :
Fe-oleate seedlayer

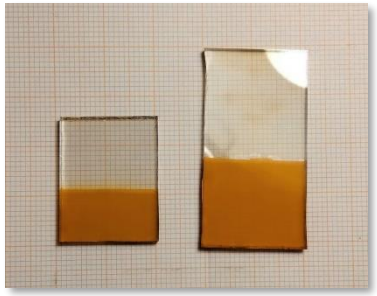

2nd step :
Hydrothermal synthesis of FeOOH

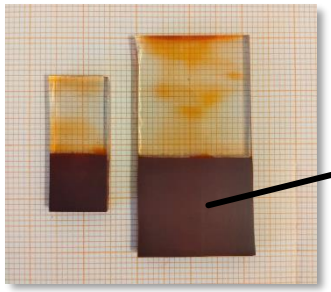

3rd step :
$TiCl_4$ doping and final annealing

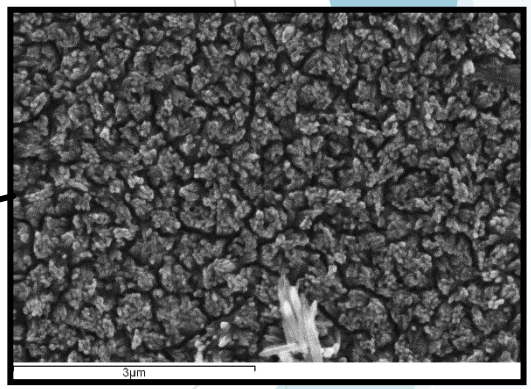

J. Deng et al., *J. Appl. Phys.*, 112, 084312, 2012

D.K. Bora, *Materials Science in Semiconductor Processing*, 31, 2015, 728–738

Hematite photoanodes for Biomass oxidation: from HMF to FDCA

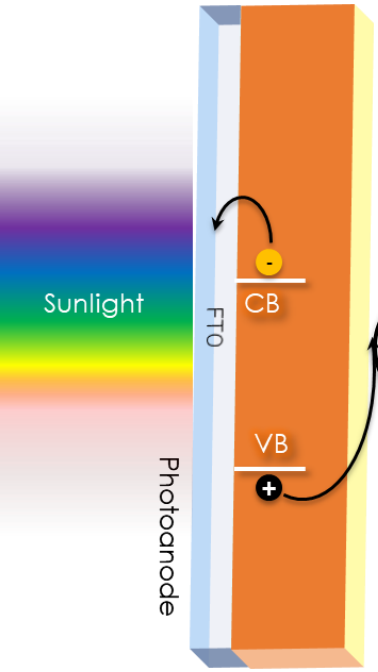

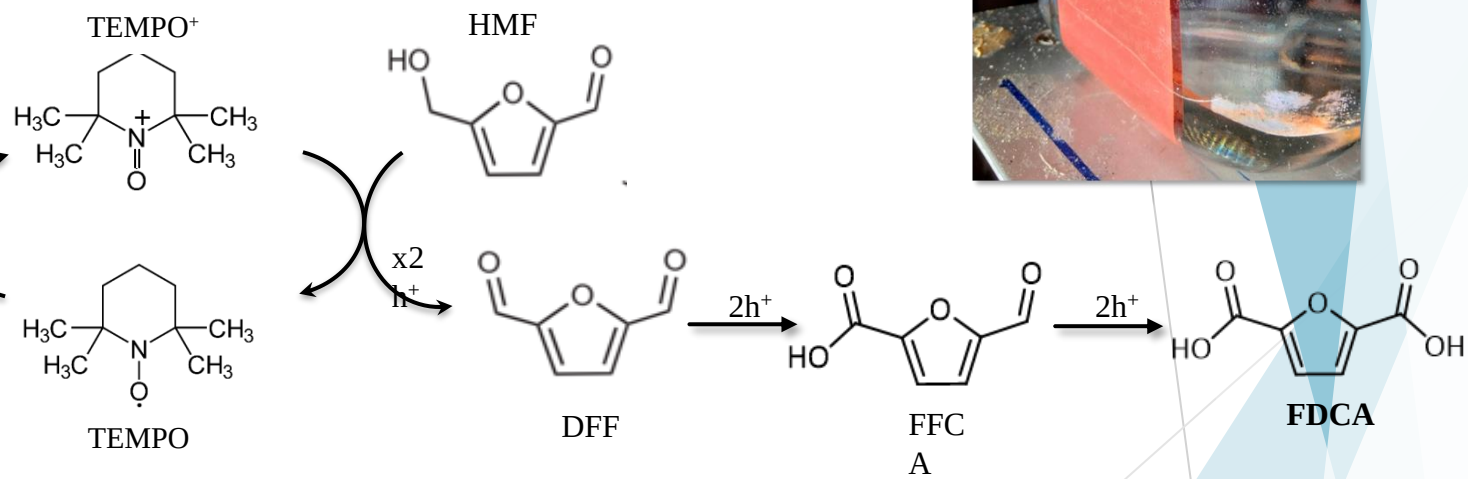

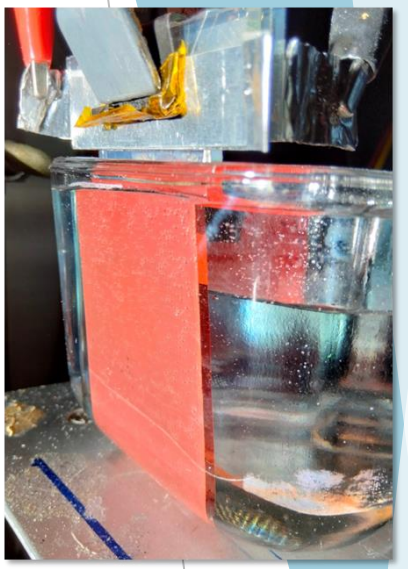

Kawde, A. et al., *Catalysts* 2021, 11, 969

J-V curves with and without TEMPO

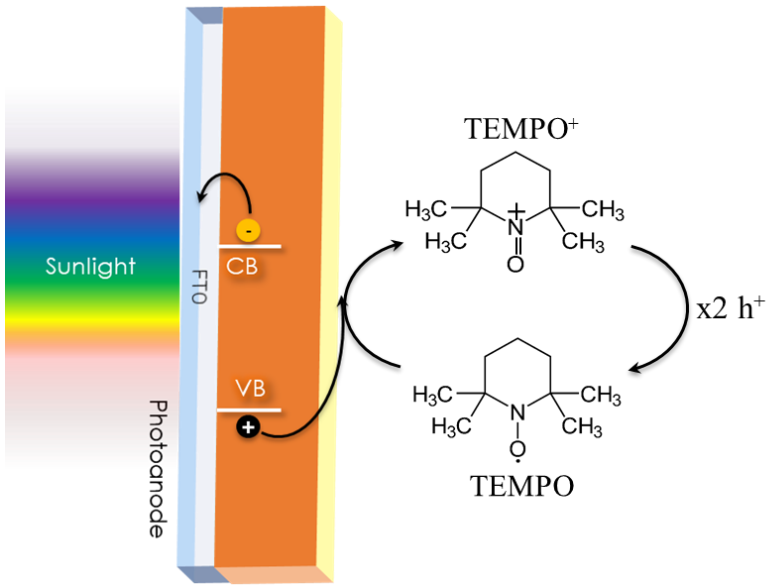

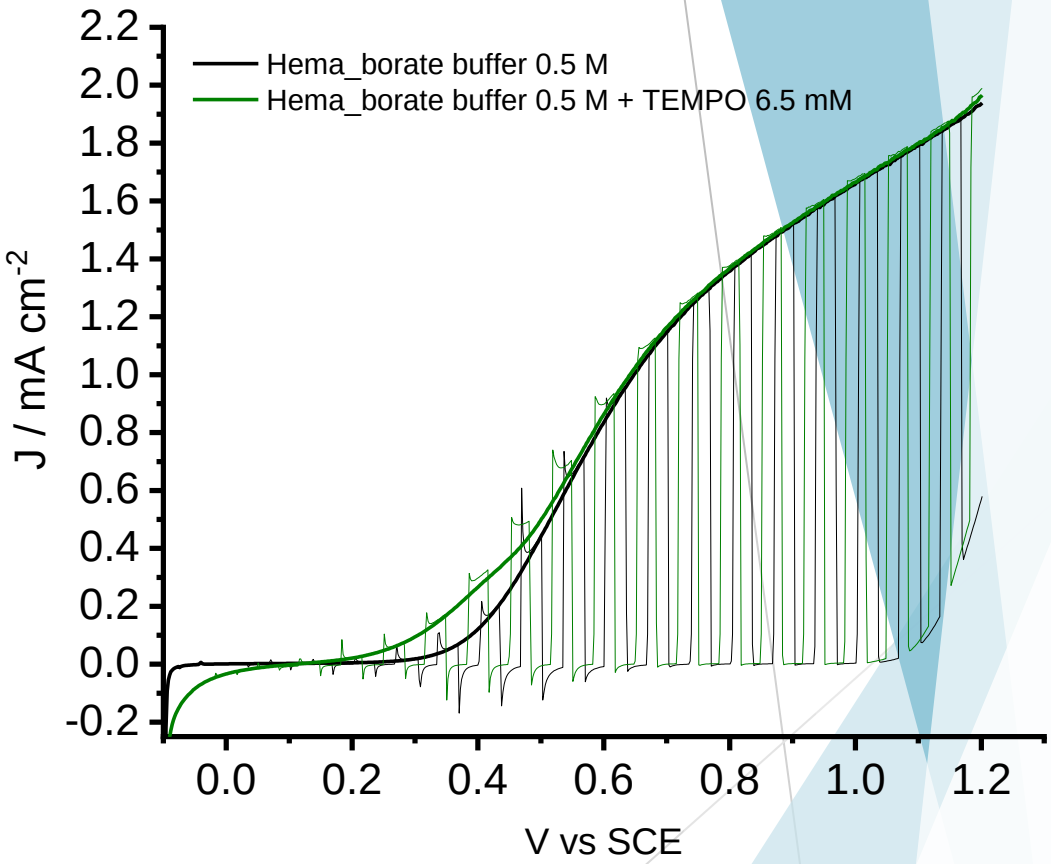

- Decreased cathodic recombination spikes in the presence of TEMPO
- Onset shifted to lower potentials

J-V curves of hematite before and after CoPi electrodeposition

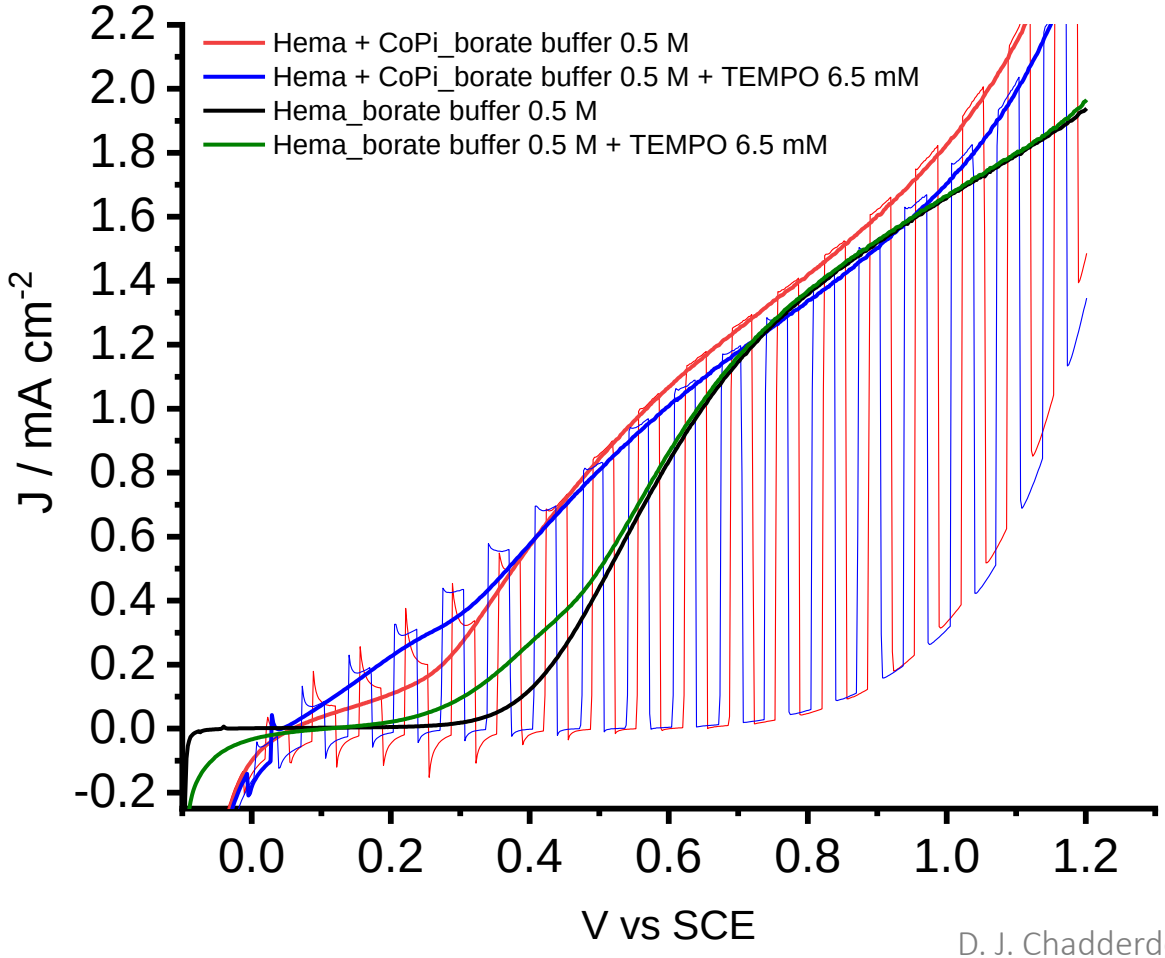

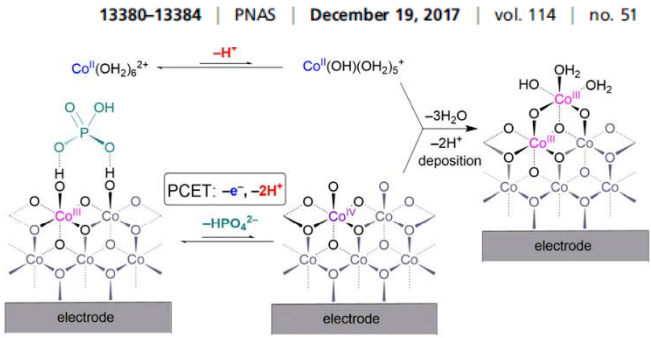

- CoPi is a cobalt(III) oxide catalyst with coordinated phosphate, known as a catalyst for water oxidation
- Significant shift of photocurrent onset and decrease of cathodic spikes in the presence of TEMPO

D. J. Chadderdon et al., ChemElectroChem, 2019, 6, 3387–3392

Electrochemical Impedance Spectroscopy of Hematite with CoPi catalyst

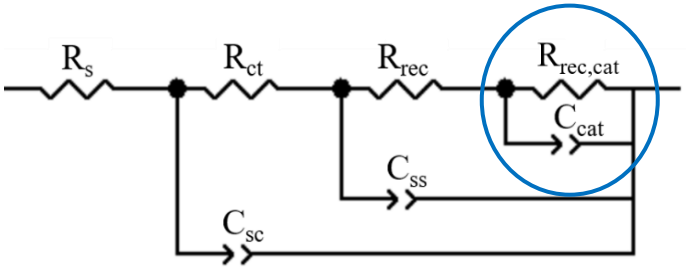

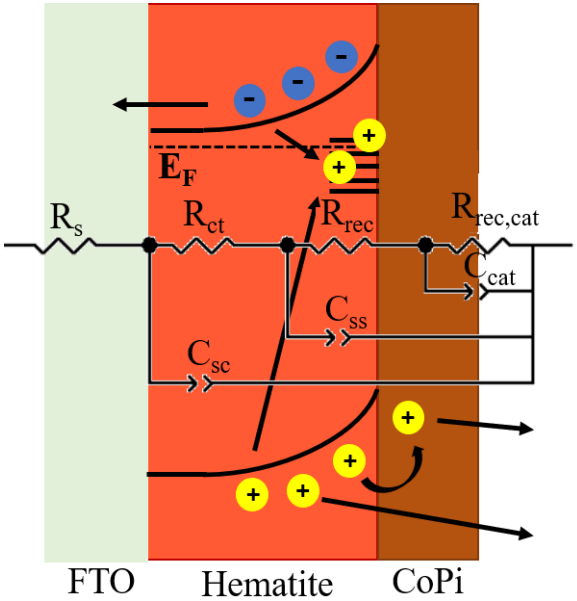

Additional mesh to account for charge transfer through the CoPi layer.
Holes trapped in Hema's SS are transferred to the CoPi layer, which subsequently transfers them to the electrolyte

Rrec,cat = recombination resistance through CoPi
Ccat = capacitance associated to CoPi

$R_{tot} = R_s + R_{ct} + R_{rec} + R_{rec,cat}$

$R_s = R_{series}$
$R_{ct} = R_{charge\ transfer}$
$R_{rec} = R_{recombination}$
$R_{rec,cat} = R_{recombination\ from\ cat}$

$C_{sc} = C_{space\ charge}$
$C_{ss} = C_{surface\text{-}states}$
$C_{cat} = C_{catalyst}$

Hema with CoPi: **Borate buffer** vs **borate buffer+TEMPO**

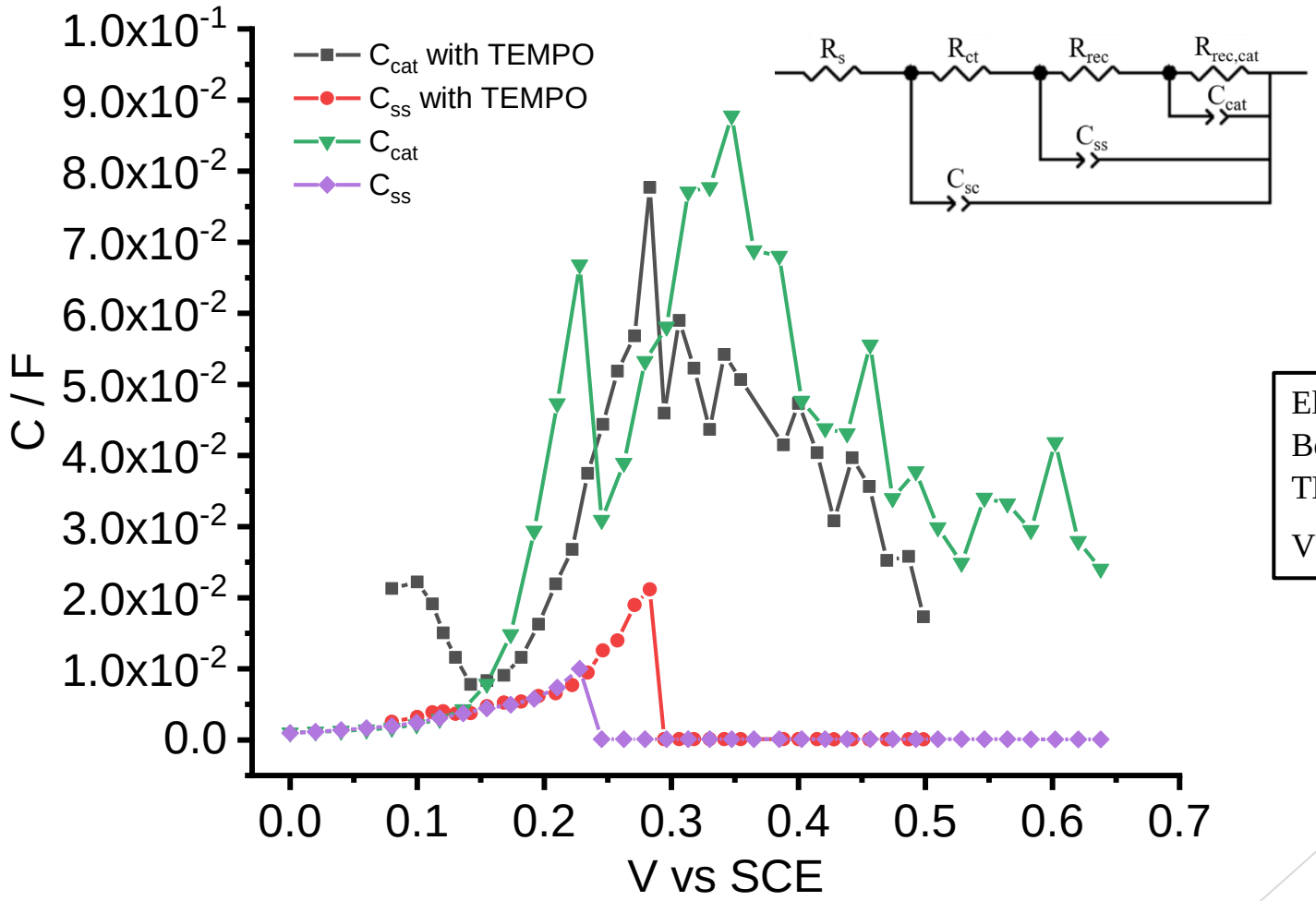

$R_{tot} = R_s + R_{ct} + R_{rec} + R_{rec,cat}$

$R_s = R_{series}$
$R_{ct} = R_{charge\ transfer}$
$R_{rec} = R_{recombination}$
$R_{rec,cat} = R_{recombination\ from\ cat}$

$C_{sc} = C_{space\ charge}$
$C_{ss} = C_{surface\text{-}states}$
$C_{cat} = C_{catalyst}$

Electrolytes:
Borate buffer 0,5 M pH 9 + TEMPO 6,5 mM

$V = V_{appl} - i\ R_s$

Conversion of HMF into FDCA

Because of the competition with OER, a full conversion of HMF to FDCA is not reached.

The presence of CoPi onto the hematite surface seems to increase the selectivity towards FDCA.

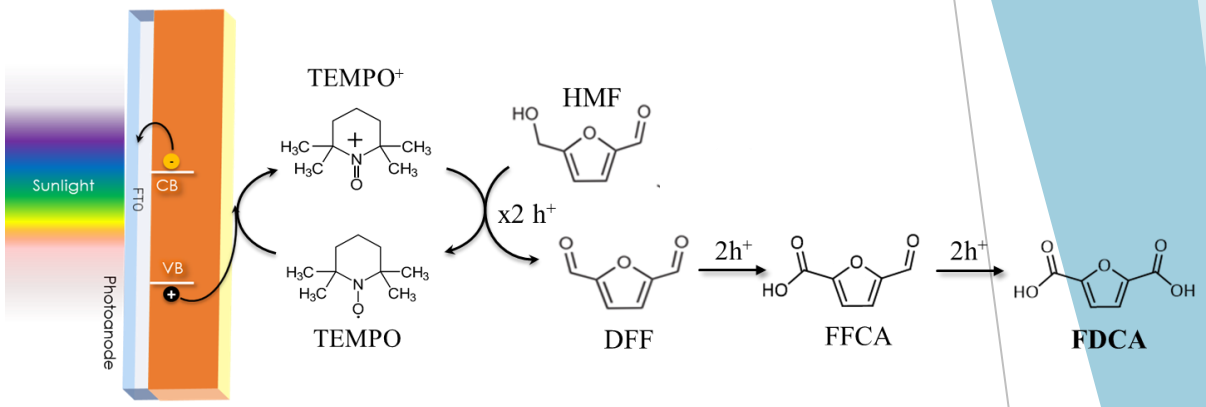

Electrode	Time of the exp (h)	Total charge passed (C)	HMF consumed (%)	Conv HMF exp in DFF (%)	Conv HMF exp in FFCA (%)	Conv HMF exp in FDCA (%)	Faradaic efficiency for FFCA+FDCA (FE%)
Hema+CoPi	18	117	100	0	31	73	**70**
Hema+CoFeOx	18	110	100	0	51	56	**75**
Hematite	19	83	100	0	57	43	**89**

Sol-Gel Routes to transparent WO_3 electrodes

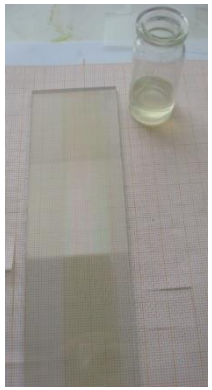

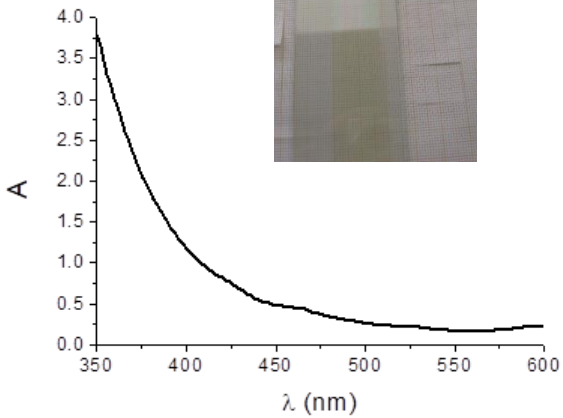

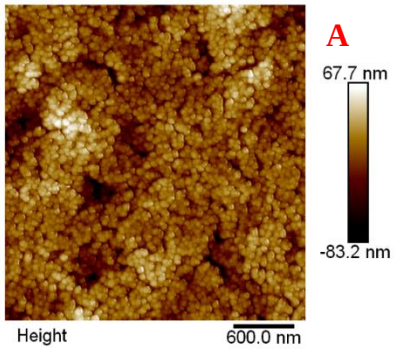

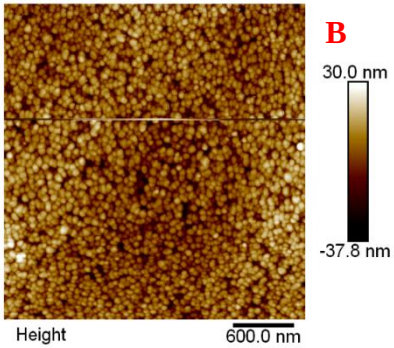

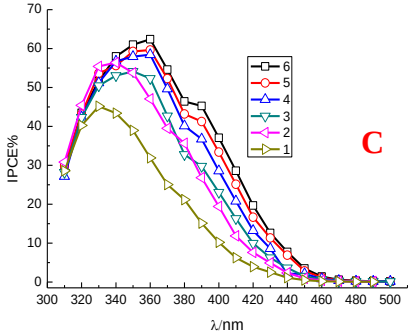

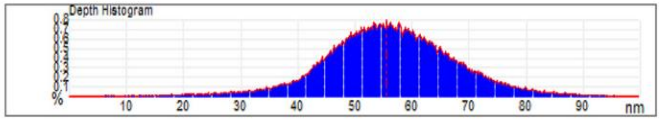

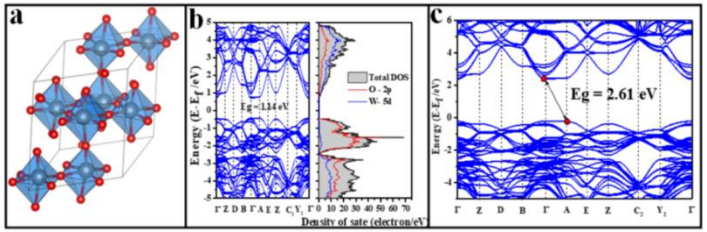

$$Na_2WO_4 + 2\ HCl \rightarrow H_2WO_4 + 2\ NaCl$$

$$H_2WO_4 \rightarrow WO_3 + H_2O$$

C. Santato, M. Odziemkowski, M. Ulmann and J. Augustynski, *JACS* 2001, **123**, 10639-10640
C. Santato, M. Ulmann and J. Augustynski, *J.Phys.Chem.B*, 2001, **105**, 936-940
R. Solarska, B. D. Alexander and J. Augustynski, *J.Solid State Electrochem.* 2004, **8**, 748-756
L. Meda, G. Tozzola, A. Tacca, G. L. Marra, S. Caramori, V. Cristino and C. A. Bignozzi, *Sol. Energy Mater. and Sol. Cells* 2010, **94**, 788-796


Solar Energy

Modular stand-alone photoelectrocatalytic reactor for emergent contaminant degradation via solar radiation

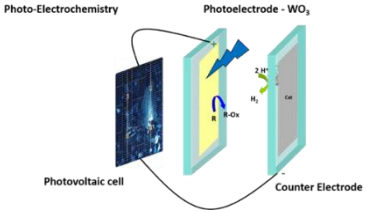

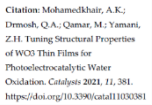
Citation: Mohamedkhair, A.K.; Drmosh, Q.A.; Qamar, M.; Yamani, Z.H. Tuning Structural Properties of WO3 Thin Films for Photoelectrocatalytic Water Oxidation. *Catalysts* 2021, *11*, 381. https://doi.org/10.3390/catal11030381


Applied Catalysis B: Environmental

journal homepage: www.elsevier.com/locate/apcatb

Photoelectrochemical mineralization of emerging contaminants at porous WO_3 interfaces

Gelsomina Longobucco, Luisa Pasti, Alessandra Molinari, Nicola Marchetti, Stefano Caramori, Vito Cristino, Rita Boaretto, Carlo Alberto Bignozzi

n-n WO_3–$BiVO_4$ heterojunctions

Electrodeposition conditions:

inally proposed by Seabold.[31] Briefly, 10 mM $VOSO_4$ in millipore water is acidified by addition of HNO_3 up to pH 0.5 followed by the addition of 10 mM $Bi(NO_3)_3$. Further HNO_3 is added until $Bi(NO_3)_3$ is completely dissolved. After this point the pH is quickly increased to 4.5 by using 2 M CH_3COONa. This solution is rapidly used (to avoid excessive hydrolysis and precipitation of Bi^{3+} compounds) for two electrode potentiostatic electrodeposition by applying 210 mV between FTO/WO_3 and a platinum foil for 600 s at room temperature.

WO_3

Working electrode (a)

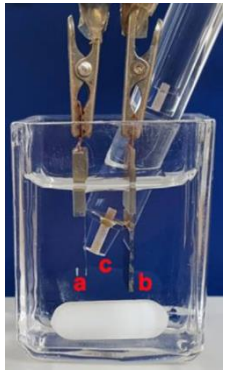

(b) Pt counter
(c) Reference

Thermal annealing

WO_3-$BiVO_4$

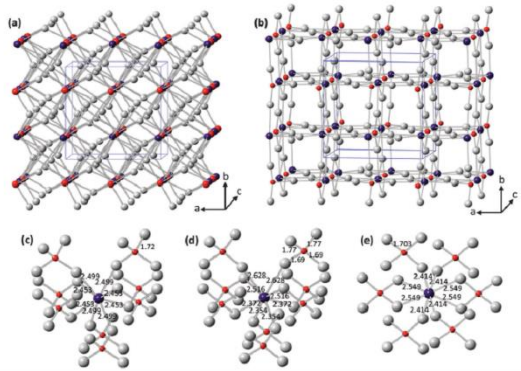

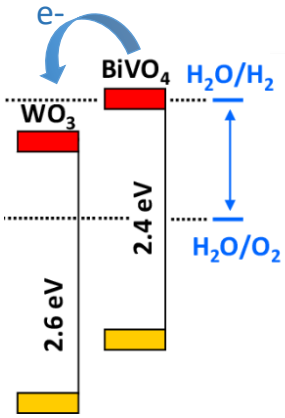

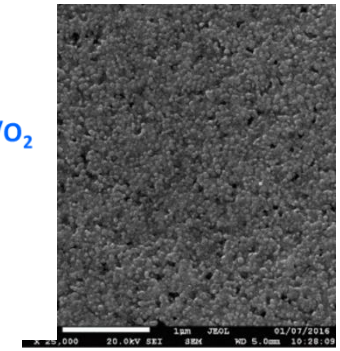

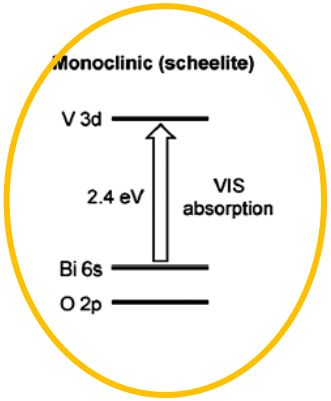

I. Grigioni et al. ***J. Phys. Chem. C*** 2015, 119, 36, 20792−20800

Park, Y.; McDonald, K. J.; Choi, K.-S. Progress in Bismuth Vanadate Photoanodes for Use in Solar Water Oxidation ***Chem. Soc. Rev.*** *2013, 42, 2321–2337*

JACS — Article — pubs.acs.org/JACS

Efficient and Stable Photo-Oxidation of Water by a Bismuth Vanadate Photoanode Coupled with an Iron Oxyhydroxide Oxygen Evolution Catalyst

Jason A. Seabold and Kyoung-Shin Choi*

dx.doi.org/10.1021/ja209001d | *J. Am. Chem.Soc.* 2012, 134, 2186–2192

Photochemical & Photobiological Sciences

PAPER

Check for updates

Cite this: *Photochem. Photobiol. Sci.*, 2019, 18, 2150

Photoelectrocatalytic degradation of emerging contaminants at WO_3/$BiVO_4$ photoanodes in aqueous solution†

Vito Cristino,[a] Luisa Pasti,[*b] Nicola Marchetti,[a] Serena Berardi,[a] Carlo Alberto Bignozzi,[a] Alessandra Molinari,[a] Francesco Passabì,[a] Stefano Caramori,[a] Lucia Amidani,[b] Michele Orlandi,[c] Nicola Bazzanella,[c] Alberto Piccioni,[d] Jagadesh Kopula Kesavan,[d] Federico Boscherini[d] and Luca Pasquini[d]

Performances of n-n WO_3–$BiVO_4$ heterojunctions

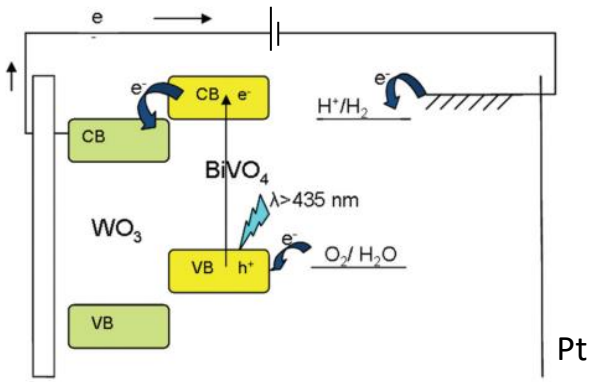

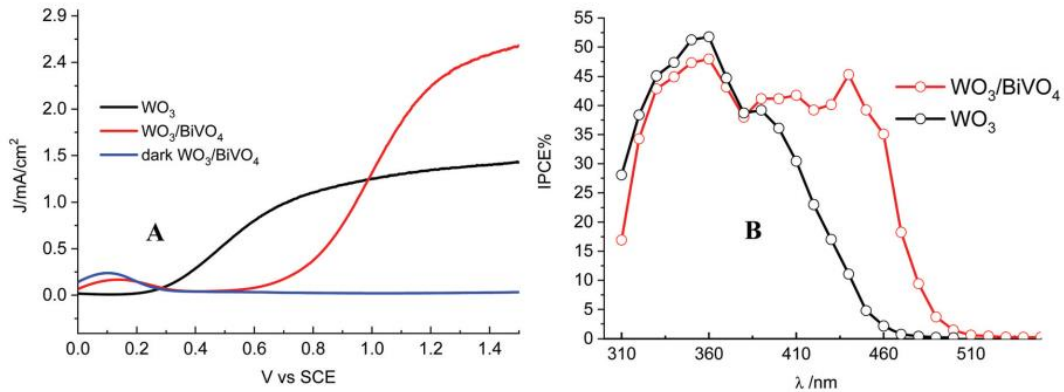

Fig. 5 (A) *J/V* curves of $WO_3/BiVO_4$ compared to those of WO_3 under 0.1 W cm^{-2} AM 1.5 G illumination. (B) Comparative IPCE spectra taken at 1.5 V *vs.* SCE. In this case front side (from the electrolyte) illumination was adopted; 0.5 M Na_2SO_4 at pH 7.

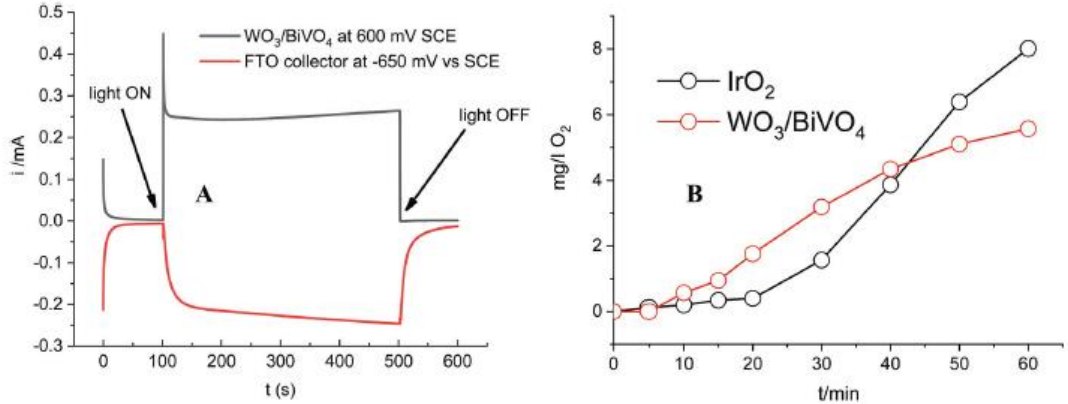

Fig. 7 (A) Oxygen detection with a generator/collector assembly, where the oxygen generator is the $WO_3/BiVO_4$ photoanode. (B) Bulk oxygen detection under prolonged galvanostatic (J = 0.5 mA cm^{-2}) photoelectrolysis, compared to an IrO_2 electrode biased at the same current.

Photochemical & Photobiological Sciences

PAPER

Check for updates

Cite this: Photochem. Photobiol. Sci., 2019, 18, 2150

Photoelectrocatalytic degradation of emerging contaminants at $WO_3/BiVO_4$ photoanodes in aqueous solution†

Vito Cristino,[a] Luisa Pasti,[*a] Nicola Marchetti,[a] Serena Berardi,[a] Carlo Alberto Bignozzi,[a] Alessandra Molinari,[a] Francesco Passabì,[a] Stefano Caramori,[a] Lucia Amidani,[b] Michele Orlandi,[c] Nicola Bazzanella,[c] Alberto Piccioni,[d] Jagadesh Kopula Kesavan,[d] Federico Boscherini[d] and Luca Pasquini[d]

ACS APPLIED MATERIALS & INTERFACES
Research Article
Cite This: ACS Appl. Mater. Interfaces 2017, 9, 37671-37681
www.acsami.org

Cobalt Hexacyanoferrate on $BiVO_4$ Photoanodes for Robust Water Splitting

Franziska Simone Hegner,[†] Isaac Herraiz-Cardona,[‡] Drialys Cardenas-Morcoso,[‡] Núria López,[*,†] José-Ramón Galán-Mascarós,[*,†,§] and Sixto Gimenez[*,‡]

ACS Energy Letters
Cite This: ACS Energy Lett. 2019, 4, 337−342
http://pubs.acs.org/journal/aelccp

Unraveling Charge Transfer in CoFe Prussian Blue Modified $BiVO_4$ Photoanodes

Benjamin Moss,[†,#] Franziska Simone Hegner,[‡,#] Sacha Corby,[†] Shababa Selim,[†] Laia Francàs,[*,†] Núria López,[*,‡] Sixto Giménez,[§] José-Ramón Galán-Mascarós,[*,‡,⊥] and James Robert Durrant[*,†]

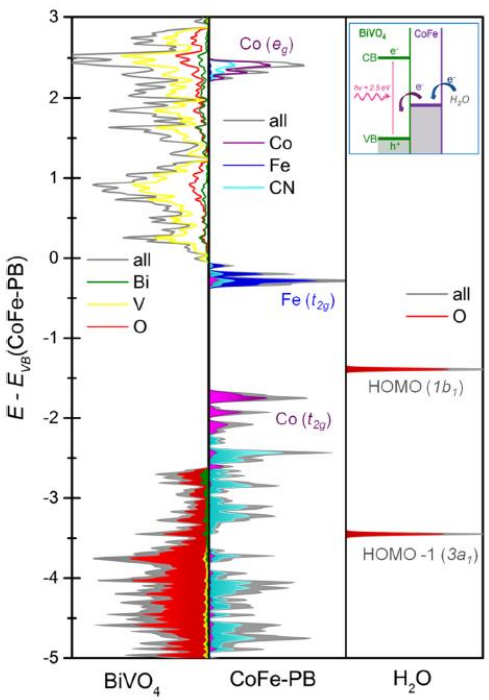

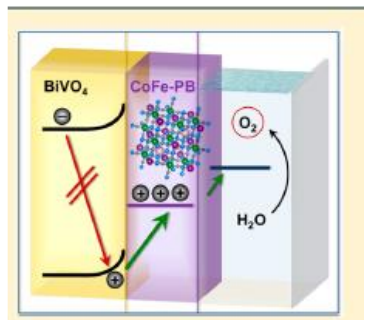

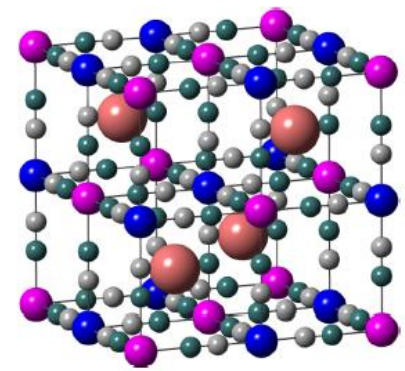

CoFe-PB

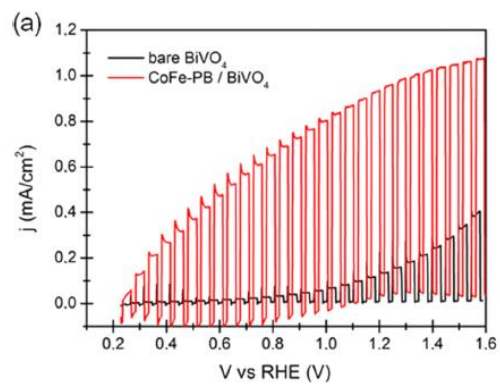

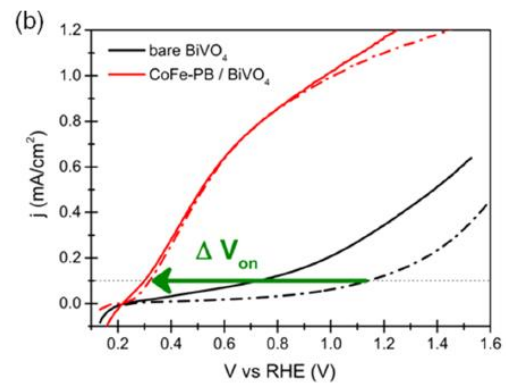

RESEARCH ARTICLE

Solar RRL
www.solar-rrl.com

Charge Separation Efficiency in $WO_3/BiVO_4$ Photoanodes with CoFe Prussian Blue Catalyst Studied by Wavelength-Dependent Intensity-Modulated Photocurrent Spectroscopy

Pierpaolo Vecchi, Alberto Piccioni, Raffaello Mazzaro, Michele Mazzanti, Vito Cristino, Stefano Caramori, and Luca Pasquini**

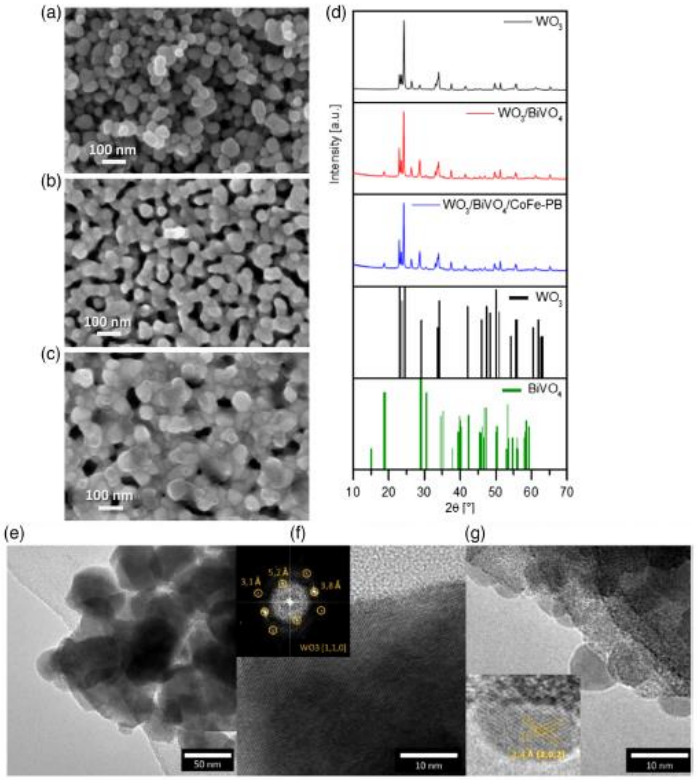

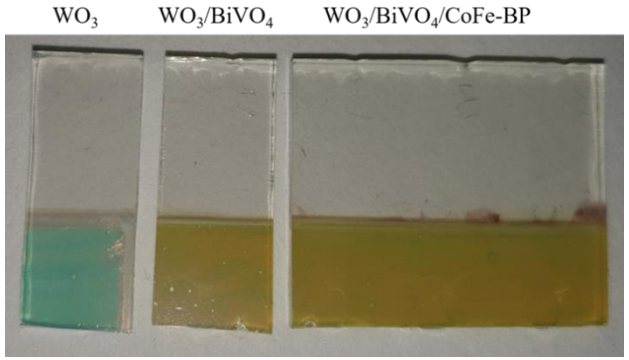

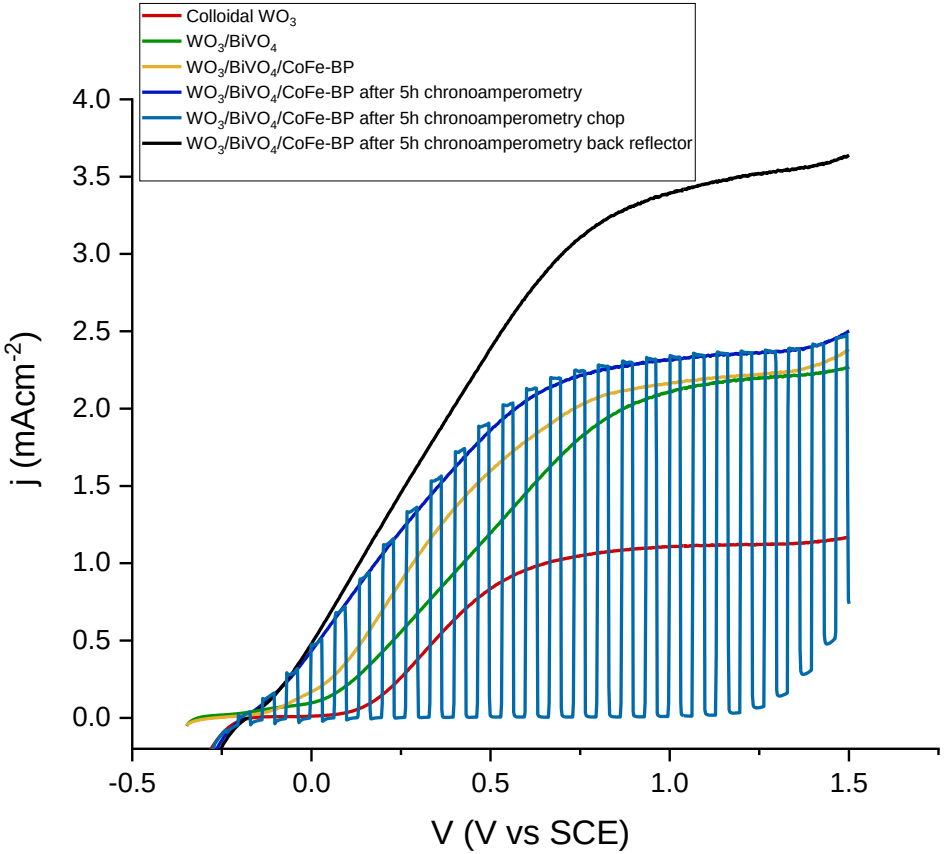

Photon to Electron Conversion Efficiency

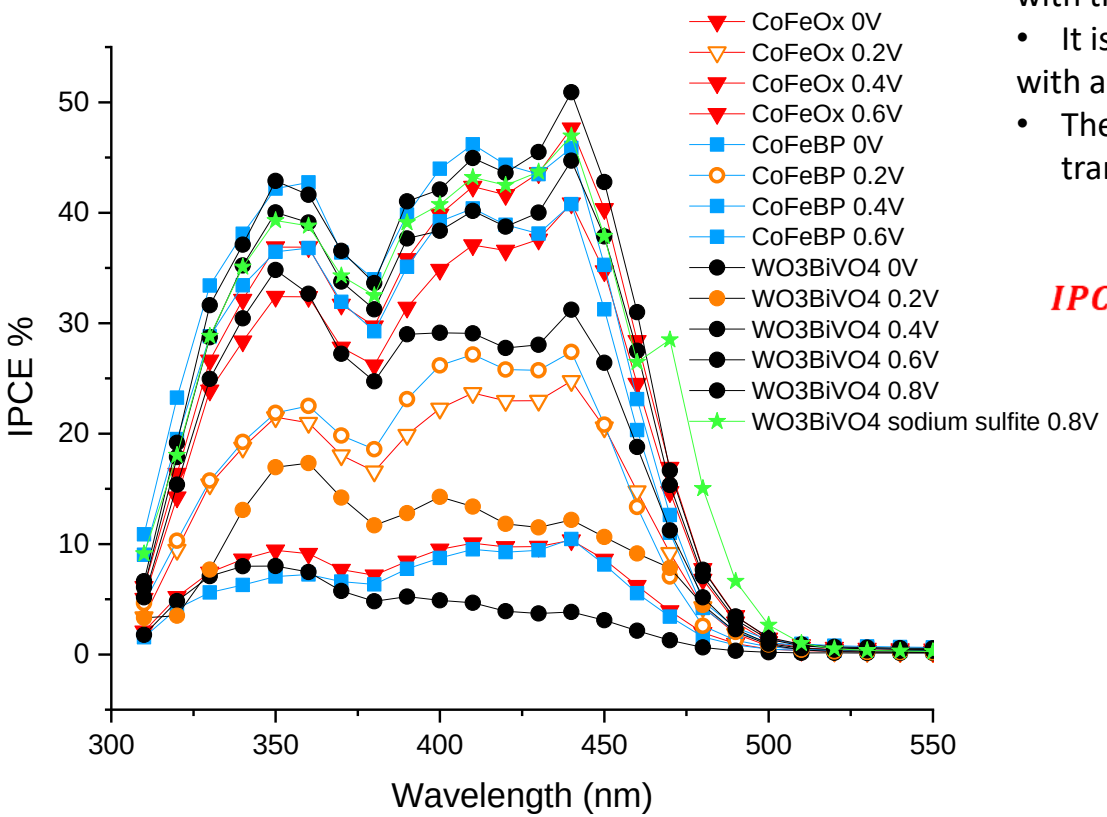

- Given sufficient bias, all photoanodes reach the same photoconversion efficiency, consistent with the limiting photocurrent density.
- It is the same maximum conversion recorded with a fast scanveger (SO_3^{2-}).
- The limiting value is thus set by the carrier transport efficiency

$$IPCE = \phi_{e/h} \times \eta_{transport} \times \eta_{interface} \times LHE$$

Transient Absorption

Transient Spectra of $WO_3/BiVO_4$ / CoFe-BP in phosphate buffer
355 nm laser excitation ca. 6mJ/cm²/pulse

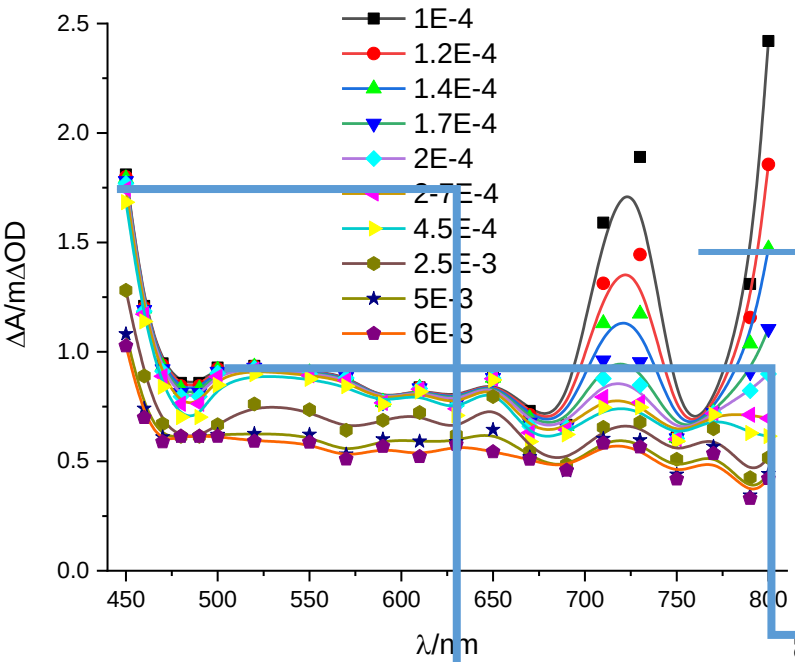

Spectroelectrochemistry of WO_3 upon cathodic Polarization

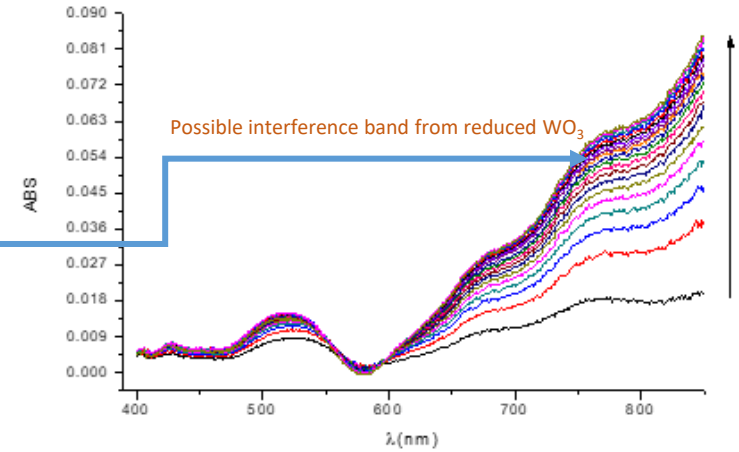

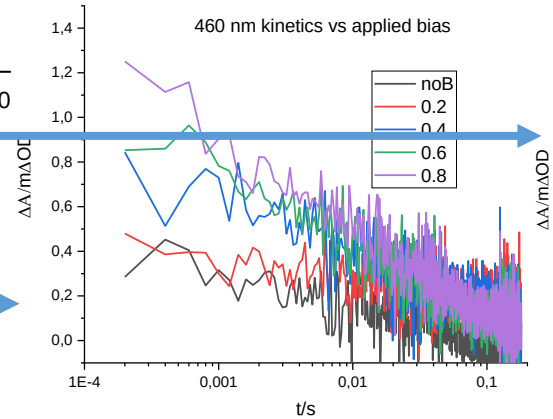

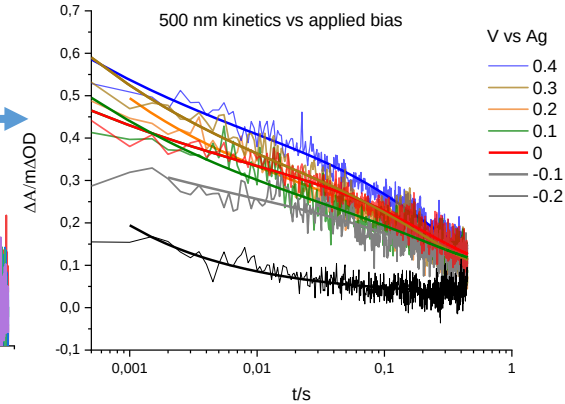

Fitting model of $BiVO_4$ photohole decay : sum of power law + KWW function

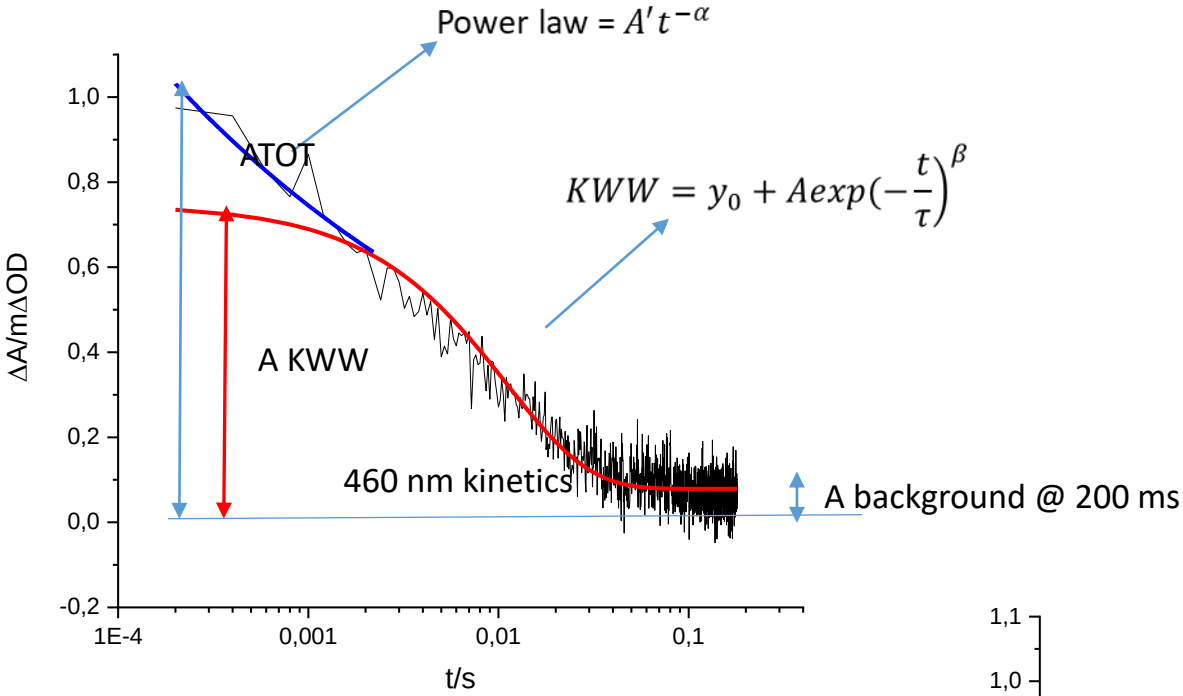

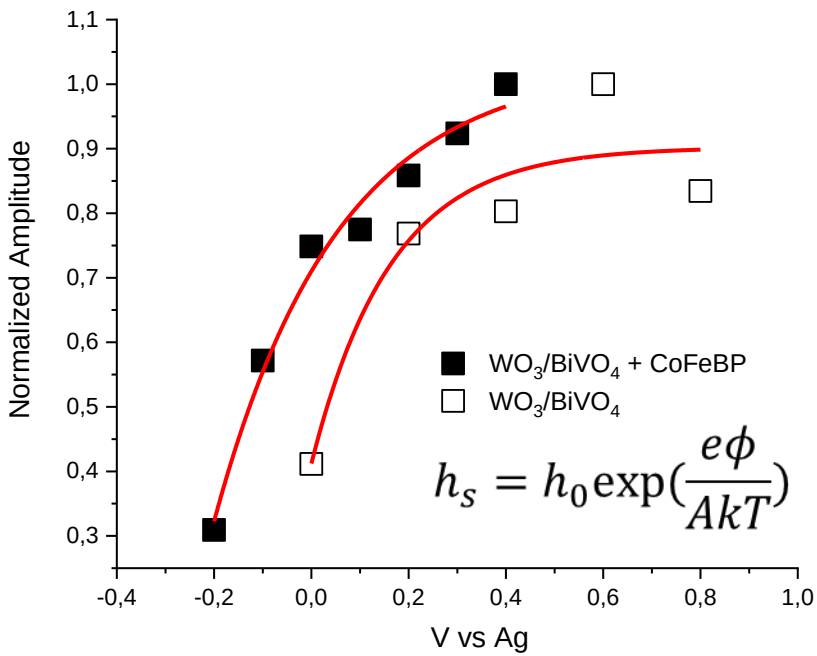

Transient Amplitudes vs photocurrent (460 nm)

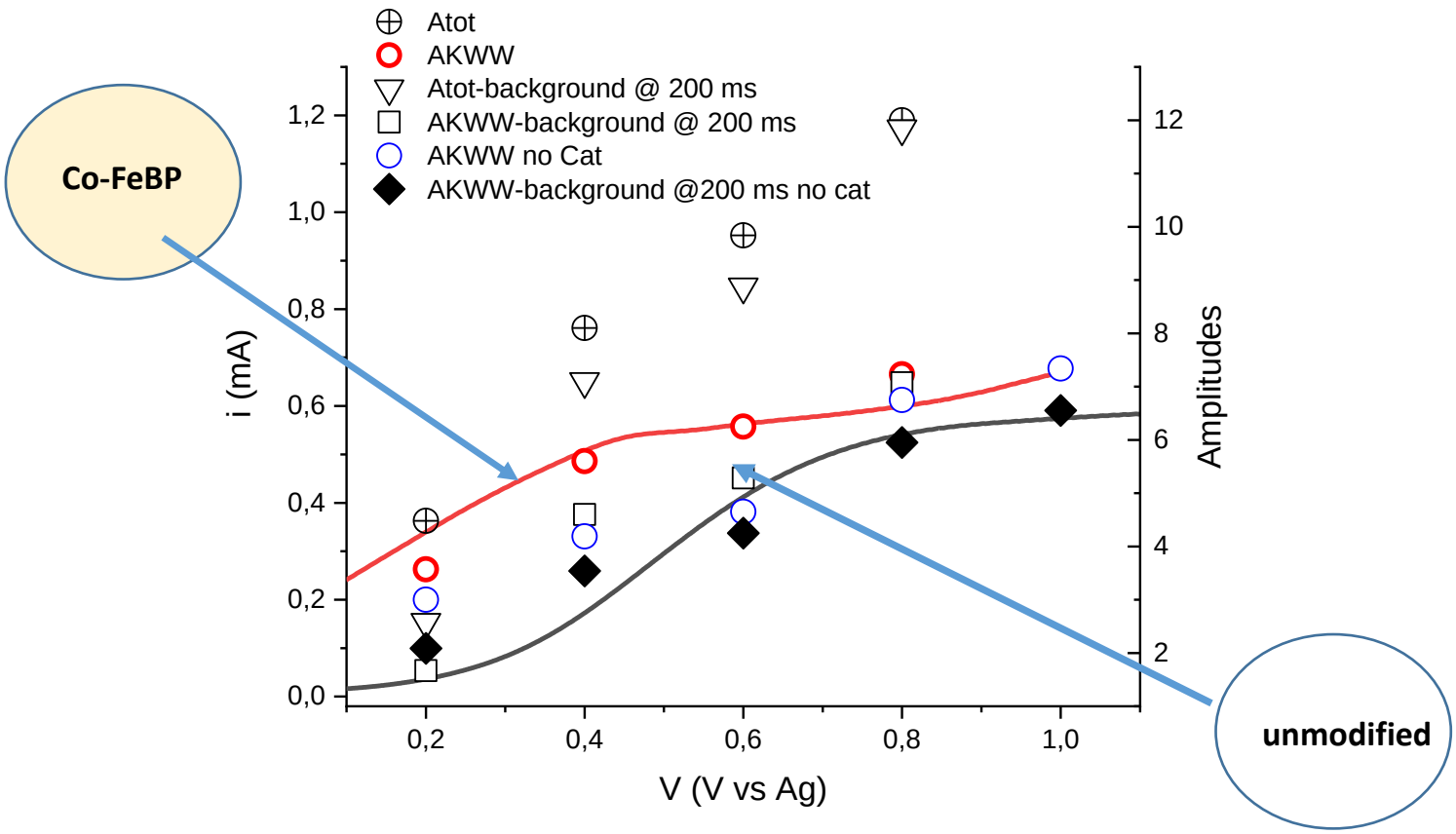

Hole Lifetime (500 nm)

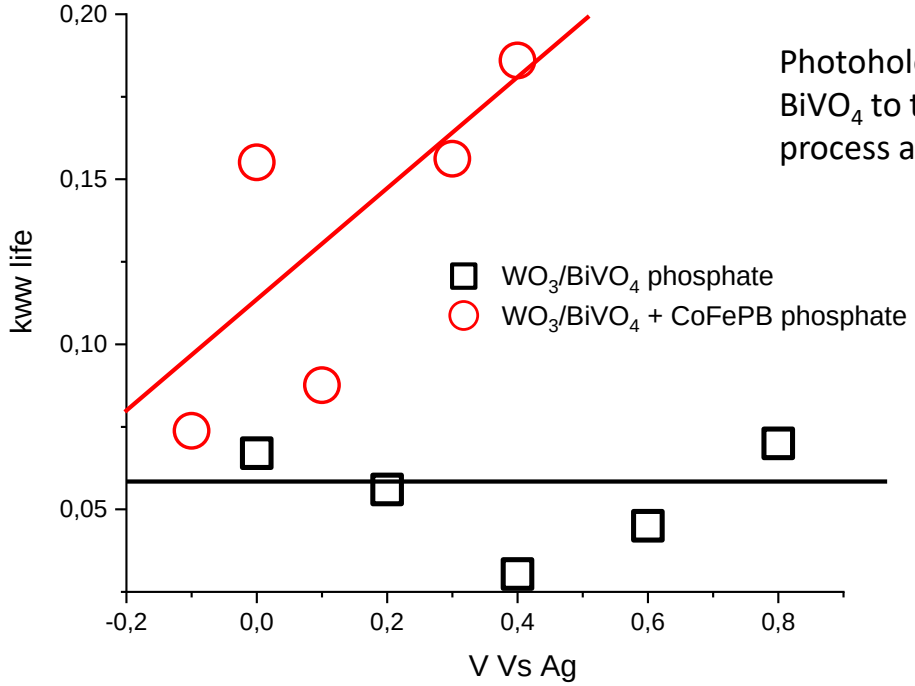

Photohole lifetime is larger when CoFePB is present. Transfer from $BiVO_4$ to the catalytic PB layer is not faster compared to the transfer process at the $BiVO_4$/phosphate interface

A look at the interfacial capacitance of $BiVO_4$

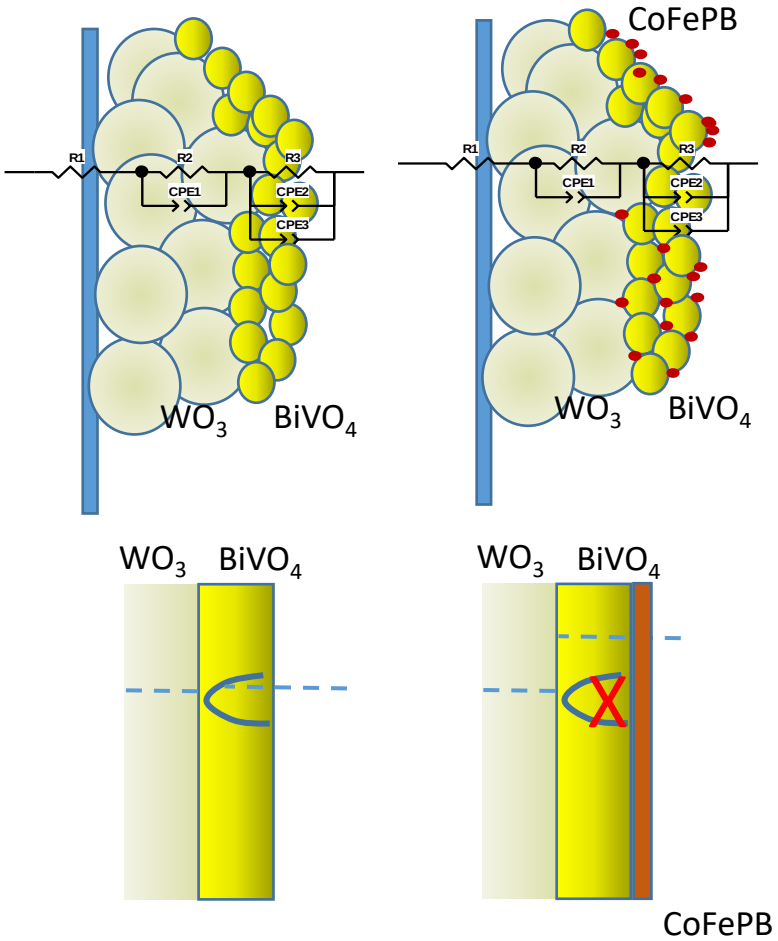

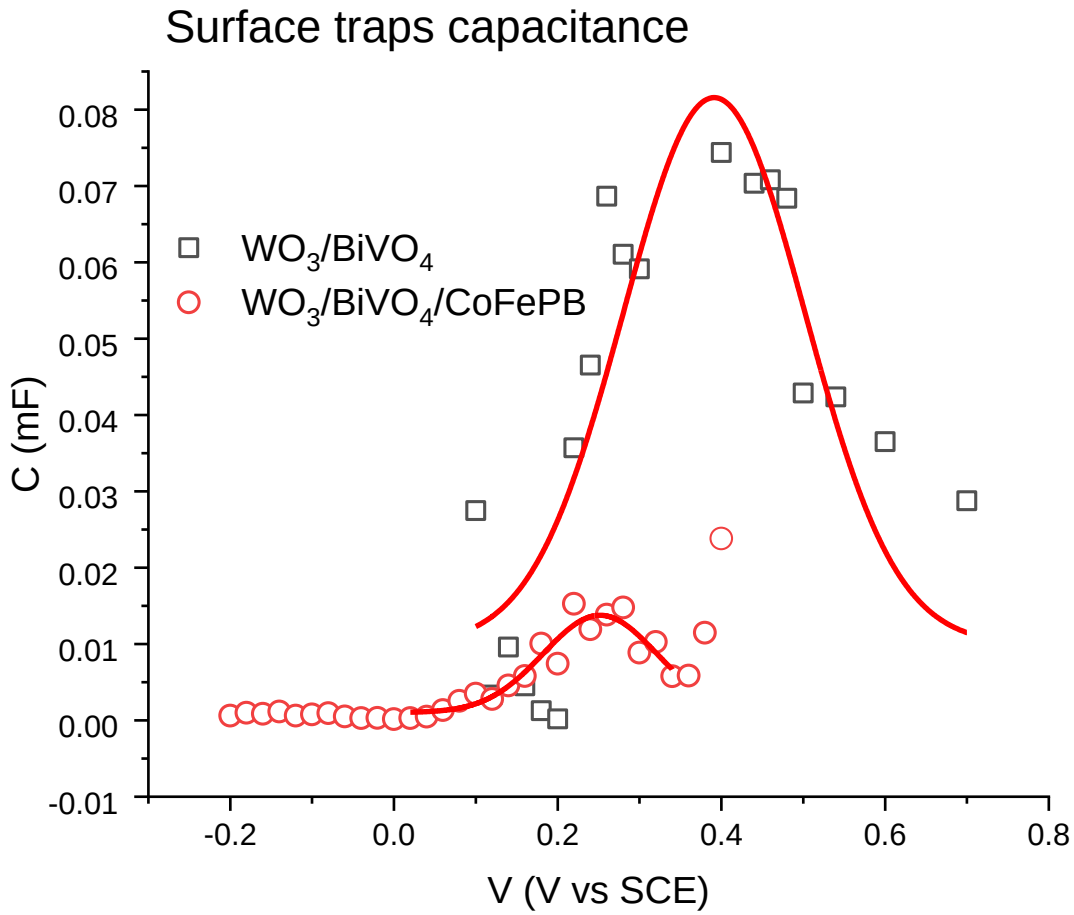

Conclusions

KWW amplitudes of photoholes are apparently related to photocurrent generation, i.e. they represent the fraction of holes that can be eventually injected in the electrolyte, escaping fast power law recombination.

The CoFe-BP catalyst allows a larger population of holes in $BiVO_4$ to survive recombination, i.e. KWW amplitudes grow faster at lower voltages compared to the unmodified junction

EIS investigation suggests that upon CoFe PB elimination of electron traps occurs, allowing the unpinning of the Fermi level of $BiVO_4$. Thus for equivalent overvoltages a deeper depletion layer achieves a better electron hole separation (hence better collection efficiency at lower voltage). The increase in photohole amplitude and lifetime is consistent with such interpretation

General Remarks

Photoelectrochemical Cells are the most direct pathway to storage of solar energy into chemical energy, ot to exploit solar power for environmental remediation processes

Some materials, particularly metal oxides, are cheap, easy to produce and display stability under photoanodic conditions in water based electrolytes. They enjoy suitable energetics to drive demanding electrochemical reactions and to harvest a sizable portion of the solar spectrum.

The thermodynamic limit for the STH of many semiconductors is still far from being achieved.
Fundamental research is still needed to understand the optimization of the interfaces, minimize recombinative losses, improve the light management, but results and progresses are being made.